https://doi.org/10.5194/egusphere-2025-2253
Preprint. Discussion started: 5 August 2025
© Author(s) 2025. CC BY 4.0 License.

# Simulated reductions in Heterogeneous Isoprene Epoxydiol Reactive Uptake from aerosol morphology in the contiguous United States using the Community Multiscale Air Quality Model (CMAQv5.3.2)

Sara L. Farrell[1], Quazi Z. Rasool[1,2], Havala O. T. Pye[3], Yue Zhang[1,4], Ying Li[5,6], Yuzhi Chen[1], Chi-Tsan Wang[1,7], Haofei Zhang[8], Ryan Schmedding[1,9], Manabu Shiraiwa[5], Jaime Green[1], Sri H. Budisulistiorini[10], Jose L. Jimenez[2], Weiwei Hu[2,11], Jason D. Surratt[1,12], and William Vizuete[1]

[1]Department of Environmental Science and Engineering, The University of North Carolina at Chapel Hill, Chapel Hill, NC, 27599
[2]Department of Chemistry and Cooperative Institute for Research in Environmental Science (CIRES), University of Colorado, Boulder, CO, USA
[3]Office of Research and Development, United States Environmental Protection Agency, Research Triangle Park, NC, 27709
[4]Now at: Department of Atmospheric Sciences, Texas A&M University, College Station, TX, 77843
[5]Department of Chemistry, University of California, Irvine, 92697, CA, USA.
[6]Now at: State Key Laboratory of Atmospheric Environment and Extreme Meteorology, Institute of Atmospheric Physics, Chinese Academy of Sciences, Beijing 100029, China
[7]Now at: Center for Spatial Information Science and Systems (CSISS), George Mason University, VA 22030
[8]Department of Chemistry, University of California, Riverside, CA 92521
[9]Department of Atmospheric and Oceanic Sciences, McGill University, Montreal, Canada, H3A 2K6
[10]Wolfson Atmospheric Chemistry Laboratories, University of York, York, UK
[11] Now at: State Key Laboratory of Organic Geochemistry, Guangzhou Institute of Geochemistry, Chinese Academy of Sciences, Guangzhou 510640, China
[12]Department of Chemistry, The University of North Carolina at Chapel Hill, Chapel Hill, NC, 27599

*Correspondence to*: Sara L. Farrell (slfarrel@live.unc.edu) and William Vizuete (vizuete@unc.edu)

**Abstract.** Aerosol particles contain complex mixtures of polar and non-polar species that can undergo organic-inorganic phase separations. In phase-separated aerosol particles, the phase state of the outer organic coating can modulate heterogeneous chemistry. Heterogeneous chemistry leading to isoprene epoxydiol (IEPOX)-derived secondary organic aerosol (IEPOX-SOA) is encoded in the Community Multiscale Air Quality (CMAQ) model and has been the focus of previous aerosol phase separation and phase state work. In a previous study, a constant ratio of water in the organic coating ($w_s$) was assumed in modeling phase separation and state. Recent studies, however, have highlighted $w_s$ as an important modulator of phase state. This work uses a later CMAQ version (version 5.3.2) with capabilities to model dynamic water uptake to the organic coating to better predict $w_s$ and its impact on the organic coating phase state. In addition, new parameterizations for estimating organic aerosol phase state were implemented in CMAQ, and the subsequent model predictions were used to compare their impacts on phase state and IEPOX-SOA predictions. These evaluations were completed simulating a summertime episode over the continental United States. Simulated diurnal profiles of aerosol phase state agreed within one standard deviation of

https://doi.org/10.5194/egusphere-2025-2253
Preprint. Discussion started: 5 August 2025
© Author(s) 2025. CC BY 4.0 License.

observationally-derived field measurements. The implementation of phase separation and phase state parameterizations, on average, decreased IEPOX reactive uptake by up to 99.99% compared to Base CMAQ, resulting in mixed model performance. While 2-methyltetrol performance improved with phase separation and phase state updates, methyltetrol sulfates and total IEPOX-SOA concentrations further underpredicted field observations in comparison to Base CMAQ.

## 1 Introduction

Fine particulate matter ($PM_{2.5}$) is a critical component of the atmosphere that can impact climate and human health both directly and indirectly (Cziczo et al., 2013; Kulmala et al., 2013; Pye et al., 2021; Tong et al., 2017). Mitigating these impacts requires knowledge of $PM_{2.5}$ composition. Organic fraction of $PM_{2.5}$ or organic aerosol (OA) is of particular interest, which, in the Northern Hemisphere, can account for up to 70% of $PM_{2.5}$ mass (Hallquist et al., 2009). Approximately 19-93% of OA is secondary organic aerosol (SOA) (Jimenez et al., 2009) which can form from the partitioning (condensation) of gas-phase organic species to existing aerosol, nucleation mechanisms, or by multiphase chemical processes (Nozière et al., 2015). SOA formation via condensation and nucleation rely on functionalization chemistry that reduces the volatility of gas-phase precursors (Donahue et al., 2006; Odum et al., 1996; Pankow, 1994). Gas-phase SOA precursor species can also dissolve into existing aqueous aerosols and cloud droplets and undergo aqueous-phase oxidation leading to lower volatility species - known as multiphase and/or heterogeneous chemistry (Eddingsaas et al., 2010; Jang et al., 2002; Kurtén et al., 2016; McNeill, 2015; Surratt et al., 2010; Zhang et al., 2018b; Zhang et al., 2019a).

The isoprene epoxydiol (IEPOX) is an isoprene-oxidation product that has been found to participate in heterogeneous formation of SOA (Gaston et al., 2014; Riedel et al., 2016; Surratt et al., 2010). IEPOX-SOA is an important source of SOA (Jo et al., 2021) as its precursor, isoprene, is estimated to be the most abundantly emitted non-methane volatile organic compound (VOC) globally (Guenther et al., 2006; Guenther et al., 2012; Sindelarova et al., 2014). In atmospheres that have higher hydrogen oxides ($HO_x$ = OH + $HO_2$) than nitric oxide (NO) concentrations, the formation of IEPOX is favored in comparison to other isoprene SOA intermediates (Lin et al., 2013; Paulot et al., 2009; Surratt et al., 2010). IEPOX-SOA formation has been found to be self-limiting (Riva et al., 2019; Zhang et al., 2019a). Scanning electron microscopy images have indicated that OA, including IEPOX-SOA, can phase separate into organic-rich and inorganic-rich phases (Riva et al., 2019; Zhang et al., 2019a), and this phase separation can limit IEPOX reactive uptake (Gaston et al., 2014; Zhang et al., 2018b). Field campaigns and chamber studies have also found that IEPOX-SOA species with higher volatilities (2-methyltetrols and $C_5$-alkene triols) can have some fraction remaining in the particle phase instead of fully off-gassing due in part to their in-particle formation from the decomposition of oligomeric species by heterogeneous OH oxidation (Armstrong et al., 2022; Hu et al., 2016; Yan et al., 2023). Hu et al. (2016) noted that IEPOX-SOA species with higher volatilities (like 2-methyltetrols and C5 alkene triols) should off-gas, however when relative humidity (RH) was less than 60%, IEPOX-SOA

https://doi.org/10.5194/egusphere-2025-2253
Preprint. Discussion started: 5 August 2025
© Author(s) 2025. CC BY 4.0 License.

mass loss to heterogeneous OH oxidation at this RH was largely less than other higher RH regimes until exposures were ≥ $10^{12}$ mol-s/cm$^3$ (Hu et al., 2016). Armstrong et al. (2022) also found with heterogeneous OH oxidation, that there was minimal loss of 2-methyltetrols from IEPOX-SOA, suggesting it could be attributed to viscous organic coatings formed that limit off-gassing (Armstrong et al., 2022). Accounting for phase separation and the phase state of outer organic coatings is paramount to constraining the formation of IEPOX-SOA and its lifetime against heterogeneous OH oxidation.

Modeling of IEPOX-SOA heterogeneous formation has evolved over the years (Budisulistiorini et al., 2017; Pye et al., 2013; Schmedding et al., 2019), with recent attention turned to exploring the impacts of phase separation and phase state on IEPOX reactive uptake (Chen et al., 2024; Gaston et al., 2014; Octaviani et al., 2021; Pye et al., 2017; Schmedding et al., 2020; Zhang et al., 2023). Recently, Schmedding et al., (2020) included and tested the parametrization of a phase separation algorithm in CMAQ and found associated reductions in heterogeneous IEPOX formation coinciding with diffusional limitations in the organic coating (Schmedding et al., 2020). Recent box modeling of chamber experiments including phase separation found the impacts of phase separation to be sensitive to diffusional limitations in the organic coating (Chen et al., 2024). In both of these studies diffusional limitations were attributed mostly to the phase state of the organic coating (Chen et al., 2024; Schmedding et al., 2020) consistent with experimental findings (Zhang et al., 2018b; Zhang et al., 2019a).

To account for phase state of the outer organic coating, Schmedding et al., (2020) made use of Shiraiwa et al., (2017)'s glass transition temperature ($T_g$) equation (which has been used as a proxy for phase state in previous studies (DeRieux et al., 2018; Koop et al., 2011). In this study, CMAQ estimated $T_g$ for each individual OA species was calculated from encoded oxygen-to-carbon ratios ($O:C$) and molar masses ($M$) of modeled OA species (Schmedding et al., 2020). Individual modeled OA $T_g$ values were then aggregated by mass fraction along with the mass fraction of water associated with the organic coating ($w_s$) to calculate the overall phase state of the organic coating ($T_g(w_{org})$) assuming ideal mixing (Chen et al., 2023). Although it has been reported that the amount of $w_s$ is a significant influence on the phase state (Lilek et al., 2022; Rasool et al., 2021), in this study, the authors had to assume the unlikely condition that 10% of all water uptake onto fine aerosol was in the organic coating using CMAQv5.2.1 as this version only tracked aerosol liquid water (ALW) associated with inorganic aerosols (Schmedding et al., 2020). Despite this assumption, the predicted particle phase state agreed within uncertainty with observationally-derived phase state data from the Centreville, Alabama, supersite during the 2013 SOAS campaign, although predicting a less viscous phase state than observed (Schmedding et al., 2020; Zhang et al., 2018a). Recently, starting with CMAQv5.3.2, OA hygroscopicity parameters ($\kappa_{org}$) - which dictate the amount of water that can be taken up by oxygenated OA - have been encoded allowing for more precise predictions of OA phase state (Pye et al., 2017). Another factor that can potentially impact the estimation of the organic coating phase state is the equation used to determine OA $T_g$ – which has yet to be systematically compared.

https://doi.org/10.5194/egusphere-2025-2253
Preprint. Discussion started: 5 August 2025
© Author(s) 2025. CC BY 4.0 License.

New relationships between $T_g$ and OA $M$, $O{:}C$, and saturation concentrations ($C^0$) have recently been derived and are summarized in Table 1 (Li et al., 2020; Zhang et al., 2019b). In Li et al. (2020), a $T_g$ equation was fit using a multi-linear least squares regression with $O{:}C$ and $C^0$ used as independent variables (Li et al., 2020), which can be applied to the information available with the two-dimensional volatility basis set framework (Donahue et al., 2011). This $T_g$ parameterization expanded the training data in comparison to Shiraiwa et al., (2017) by including larger molecular weight OA species and sulfated and nitrated species (Li et al., 2020; Shiraiwa et al., 2017). When this parameterization was evaluated against measured $T_g$ values, the authors reported a correlation coefficient, R = 0.93 (Li et al., 2020). Another important process influencing the phase state of an aerosol is the rate at which it is cooled (Zhang et al., 2019b). Aerosols can strengthen vertical updrafts which could potentially result in aerosols cooling at different rates (Abbott et al., 2021). In Zhang et al. (2019b), $T_g$ was measured for 13 OA species at different cooling rates and used to derive a relationship between $T_g$, $M$, temperature ($T$), and $C^0$ (Zhang et al., 2019b). In comparison to the $T_g$ equation formulated in Shiraiwa et al. (2017), these two new $T_g$ parameterizations account for heavier and more functionalized OA species and therefore warrant exploration in CMAQ (Li et al., 2020; Shiraiwa et al., 2017; Zhang et al., 2019b).

**Table 1.** The implemented glass transition temperature ($T_g$) parameterization and variables used such as molar mass ($M$), oxygen-to-carbon ratios ($O{:}C$), temperature ($T$), and saturation concentration at 298K ($C^0$). Also shown are the experimental data and fit methodology used to develop each parameterization based on carbon-hydrogen (CH), carbon-hydrogen-oxygen (CHO), carbon-hydrogen-oxygen-sulfur (CHOS), and carbon-hydrogen-oxygen-nitrogen (CHON) species.

| Label | Input Variables for Parameterization | Experimental Data | Fit Methodology |
|---|---|---|---|
| Shiraiwa (Shiraiwa et al., 2017) | $M$, and $O{:}C$ | 179 CH and CHO compounds with observed $T_g$ from previous studies | Multi-linear least squares regression |
| Zhang (Zhang et al., 2019b) | $M$, $T$, and $C^0$ | 13 CHO and CHOS compounds with experimentally found $T_g$ measured at a cooling rate of 5K/min | Exponential fit |
| Li (Li et al., 2020) | $O{:}C$ and $C^0$ | 2448 CH, CHO, CHON, and CHOS compounds with observed $T_g$ from previous studies or estimated $T_g$ from observed or estimated melting temperatures | Multi-linear least squares regression |

https://doi.org/10.5194/egusphere-2025-2253
Preprint. Discussion started: 5 August 2025
© Author(s) 2025. CC BY 4.0 License.

This study aims to explore the impacts of phase separation and phase state of the organic coating on modeled IEPOX heterogeneous reactive uptake, taking advantage of recently published $T_g$ parameterizations (Table 1) (Li et al., 2020; Shiraiwa et al., 2017; Zhang et al., 2019b). The phase state algorithms, previously used to calculate bulk OA phase state, can now take advantage of water uptake to the organic coating via $\kappa_{org}$ values released in CMAQv5.3 (Pye et al., 2017). Furthermore, this study explores the influence of modeled aerosol physical properties, such as $w_s$, $C^0$ and $O{:}C$ on organic coating phase state across parameterizations and how each compare with observational data to provide insights on OA phase state and its impact on heterogeneous SOA formation.

## 2 Methods

### 2.1 Air Quality Model Setup

CMAQ version 5.3.2 was used for this analysis with meteorological inputs and emissions files developed to support the SOAS field campaign from June 1st to July 15th, 2013, with a spatial resolution of 12 km by 12 km (Appel et al., 2020) with similar inputs used in (Schmedding et al., 2020). Meteorological inputs were predicted using the Weather Research Forecasting Model (WRF) version 3.8 with lightning assimilation (Appel et al., 2017; Heath et al., 2016). Anthropogenic emissions were sourced from the EPA's National Emissions Inventory (NEI) 2011 version 2. Biogenic emissions were predicted using the Biogenic Emissions Inventory System (BEIS) version 3.6.1, with biogenic isoprene emissions scaled up by a factor of 1.5 to better match isoprene measured at the Centreville, AL SOAS site (CTR) as detailed in (Pye et al., 2017). The State Air Pollution Research Center version 07tic with extended isoprene chemistry and aero7i treatment of SOA (SAPRC07tic_ae7i) was used as the chemical mechanism (Xie et al., 2013) as it explicitly tracks 2-methyltetrols (AIETET) and methyltetrol sulfates (AIEOS, also known as IEPOX organosulfate) (Pye et al., 2013). These are the predominant IEPOX-derived SOA species permitting the tracking of the influence of sulfate aerosols on the acid-driven multiphase chemistry (reactive uptake) of IEPOX (Budisulistiorini et al., 2015a, 2015b; Budisulistiorini et al., 2017; Pye et al., 2013).

### 2.2 Implementation of phase separation and phase state

A summary of the CMAQ algorithm used for determining phase separation and phase state are shown in Figure 1, mirroring the implementation of the "PhaseSep2" model setup documented in (Schmedding et al., 2020). As shown in Fig. 1, phase separation was determined based on the separation relative humidity (SRH) and occurs when the SRH ≥ RH (Bertram et al., 2011; You et al., 2014). The SRH was determined based on aggregated aerosol $O{:}C$ ($O{:}C_{avg}$) and organic matter to inorganic sulfate ratios ($OM{:}IN_{sulf}$) (Bertram et al., 2011; Schmedding et al., 2020; Song et al., 2018; Zuend et al., 2012). The $O{:}C$ were derived from organic matter-to-organic carbon ratio ($OM{:}OC$) using the relationship published in Simon and Bhave

https://doi.org/10.5194/egusphere-2025-2253
Preprint. Discussion started: 5 August 2025
© Author(s) 2025. CC BY 4.0 License.

(Simon et al., 2012). If phase separated, Eq. 2 (shown in Fig. 1) is used to calculate the overall $T_g$ of the organic coating with water accounted for, referred to from here-on-out as $T_g(w_{org})$, based on the composition of the aerosol and the $w_s$. The $T_g(w_{org})$:$T$ ratios were then used determine the viscosity of the organic coating ($\eta_{org}$) (Eq. 3-6 shown in Fig. 1) using a modified Vogel-Tamman-Fulcher equation (DeRieux et al., 2018; Fulcher, 1925; Schmedding et al., 2020; Tammann et al., 1926; Vogel, 1921). Equations for the viscosity of the aerosol (i.e., Eq. 3-6) and ultimately the diffusivity of IEPOX through the organic coating ($D_{org,eff}$, Eq. 7) are also provided in Fig. 1. The $D_{org,eff}$ is then used in the resistor term for IEPOX heterogeneous reactive uptake documented in the supplemental information (SI Section 1).

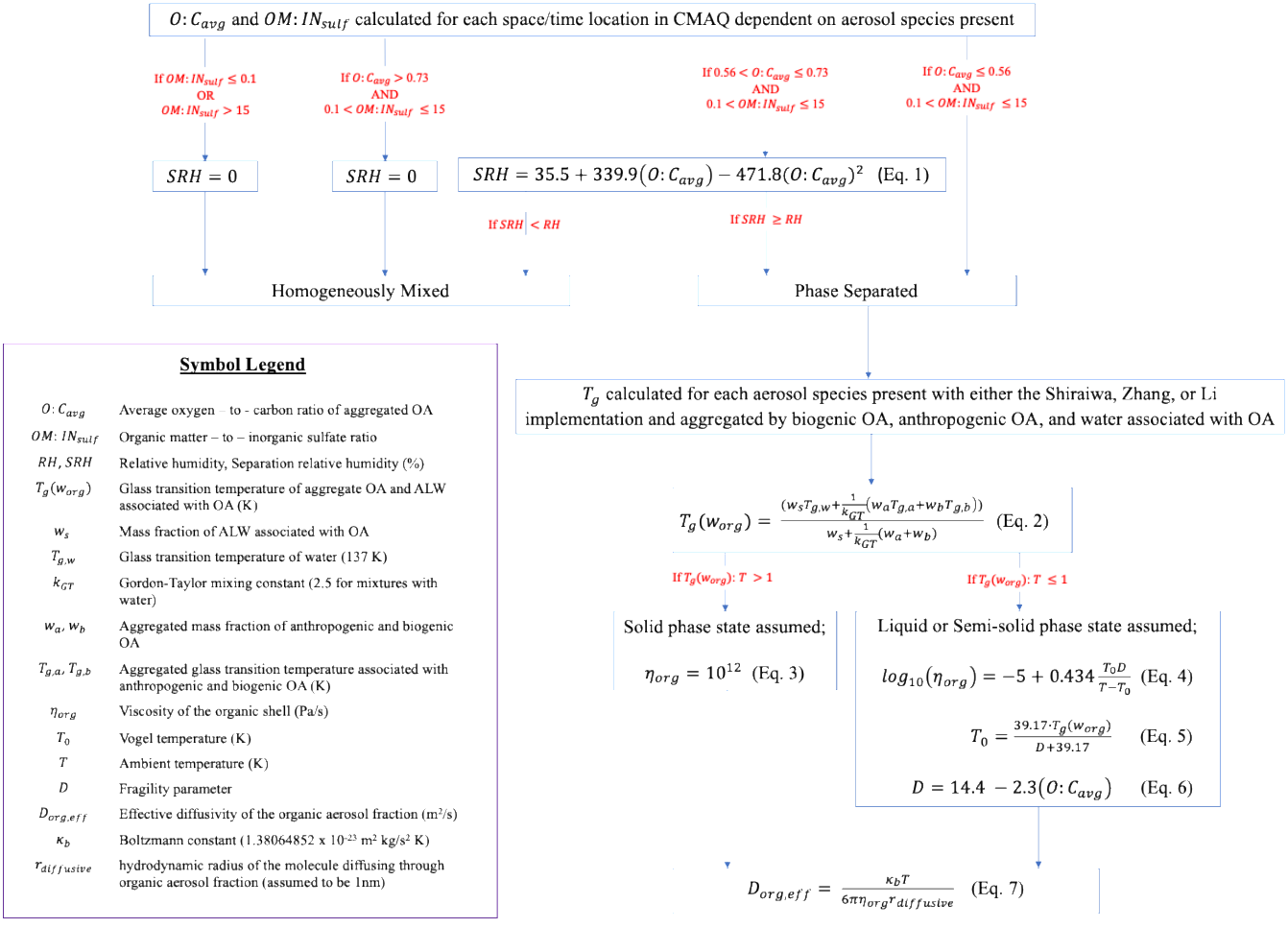


**Figure 1.** Algorithm used to determine phase separation (Bertram et al., 2011; You et al., 2013; You et al., 2014; Zuend et al., 2012) and phase state (Schmedding et al., 2020), including the parameters used to determine whether aerosol particles were in a liquid, semi-solid or solid phase state. Also shown are the equations used to determine viscosity ($\boldsymbol{\eta_{org}}$) (Fulcher, 1925; Tammann et al., 1926; Vogel, 1921) and the effective diffusivity of IEPOX through the organic coating ($\boldsymbol{D_{org,eff}}$) (Miller, 1924).

https://doi.org/10.5194/egusphere-2025-2253
Preprint. Discussion started: 5 August 2025
© Author(s) 2025. CC BY 4.0 License.

When $w_s = 0$, the aggregated OA phase state equation (Eq. 2) is equal to the mass fraction weighted aggregated $T_g$s, previously referred to as the dry phase state equation, represented by $T_{g,org}$ (Dette et al., 2014; Li et al., 2021; Li et al., 2020). Given the numerical precision of CMAQ and the likelihood of very small $w_s$ values-characteristic of dry OAs yet still greater than zero-
170 the occurrence of $w_s = 0$ was minimal. A recent publication defined the dry phase state as $w_s \leq 0.1$ (Rasool et al., 2021). While CMAQ does not implement conditionals to switch phase state equations based off $w_s$ values, we identify dry aerosol phase state instances offline using this threshold and refer to it as $T_{g,org}$.

### 2.3 CMAQ Implementation of Glass Transition Temperature

175 The details of the implementation of the Shiraiwa et al. (2017) parameterization is provided in (Schmedding et al., 2020; Shiraiwa et al., 2017). The details for the implementation of the Zhang et al. (2019b) and Li et al. (2020) parameterizations are provided below.

#### 2.3.1 Zhang parameterization

A logarithmic relationship between the relaxation time of an aerosol species and inverse temperature has been established in
180 (Zhang et al., 2018). Using this relationship, Zhang et al. (2019b) explored the implication of cooling rates on $T_g$ values. Ultimately, a cooling rate of 5 K/min was determined to be the most atmospherically-relevant cooling rate for calculating the $T_g$ values of individual aerosol species using the Zhang et al. (2019b) parameterization ($T_{g,i,Z}$) at average atmospheric conditions. Thirteen measured $T_{g,i,Z}$ values were then related to saturation concentrations predicted using the EVAPORATION model (Compernolle et al., 2011) and the following equation (Zhang et al., 2019):

185

$$T_{g,i,Z} = 480.071 - \frac{54395}{(log_{10}\left(\frac{RT}{M10^6}C^0\right)-1.7929)^2+116.49} \quad (8)$$

Where $R$ is the ideal gas law constant (8.2 x $10^{-5}$ $m^3$ atm/mol K), $T$ is the temperature (K), $M$ is molar mass of the organic compounds, and $C^0$ is the saturation concentration (µg/$m^3$).

#### 2.3.2 Li Parameterization

190 The Li et al. (2020) parameterization used a database of 2,448 CH, CHO, CHON, and CHOS compounds, of which 943 are sulfated and 276 are nitrogenated species. Measured $T_g$ values are available for a total of 337 compounds, with the majority (of 259) being CHO compounds. When $T_g$ measurements are not available, $T_g$ is estimated from the melting temperature ($T_m$) by applying the Boyer-Kauzmann rule of $T_g = g \times T_m$ with $g \approx 0.7$ (Koop et al., 2011), referred to as the "estimated $T_g$" (Li et al., 2020). The authors also used a test dataset of 654 CHO and 212 CHON compounds that were not included in the training

https://doi.org/10.5194/egusphere-2025-2253
Preprint. Discussion started: 5 August 2025
© Author(s) 2025. CC BY 4.0 License.

dataset. Using experimentally measured or estimated $T_g$ values for aerosol species in a multi-linear least squares analysis was completed with $C^0$ values and $O:C$ ratios, and the authors reported the following equation (Li et al., 2020):

$$T_{g,i,L} = 289.10 - 16.50 \times log_{10}(C^0) - 0.29 \times [log_{10}(C^0)]^2 + 3.23 \times log_{10}(C^0)(O:C) \quad (9)$$

This parameterization has been recently applied in a global chemical transport model GEOS-Chem and a regional air quality model WRF-Chem, providing consistent results with phase state measurements at the surface level (Luu et al., 2025; Zhang et al., 2024)

### 2.4 CMAQ Modifications for Calculation of $T_g$

The $T_g$ implementations described above require effective $C^0$ (at 298K) for all CMAQ OA species. These values are shown in Supplemental Table 1. It is important to note that some of the CMAQ low-volatility organic species (LVOS) species are assigned a nonvolatile saturation concentration ($C^0$ = $10^{-9}$ (ug/m$^3$)) to ensure that these species condense entirely, consistent with the initial default implementation (Pye et al., 2015; Pye et al., 2023). Except for dimers and oligomers, there has been evidence to suggest that some of these LVOS species, like monoterpene hydrolysis products (AMTHYD) and AIETET, may still partition back to the gas phase (Budisulistiorini et al., 2017; Kurtén et al., 2016). To avoid biasing modeled $T_g$ which depended on $C^0$ values, all LVOS that had a $C^0$ of $10^{-9}$ ug/m$^3$ were updated in CMAQ as shown in Supplemental Table 2. The process for updating started with a literature review for any reported $C^0$ or saturation vapor pressure ($p_0$) that could update the existing CMAQ species. If neither a $C^0$ nor $p_0$ was found, the chemical structure of the LVOS surrogates were referenced and their structures were coded into the Simplified Molecular Input Line Entry System (SMILES) coding notation (Anderson, 1987). Once SMILES were coded, they were input into the OPEn structure–activity/property Relationship App (OPERA) (Mansouri et al., 2018), where $p_0$ were estimated and then used to calculate $C^0$ using the following relationship assuming that the activity coefficient is 1 (Donahue et al., 2006; Pankow, 1994; Zhang et al., 2019b):

$$C^0 = \frac{M10^6 p_0}{RT} \quad (14)$$

Where $M$ is the molar mass, $R$ is the ideal gas constant ($8.2\times10^{-5}$ m$^3$ atm mol$^{-1}$ K$^{-1}$), and $T$ is the temperature. $T$ is assumed to be 300K to correspond with temperature used to derive all CMAQ $C^0$ values (Pye et al., 2017). CMAQ $M$'s were not updated to correspond with the proxy species $p_0$ and instead reflect that of derived values from the SAPRC07tic_ae7i mechanism (for conservation of mass) and represent a potential limitation of this study.

https://doi.org/10.5194/egusphere-2025-2253
Preprint. Discussion started: 5 August 2025
© Author(s) 2025. CC BY 4.0 License.

### 2.5 Observational Data

Observed $O:C$ ratios and molar masses were obtained from 800+ OA species that were measured at the Centreville, Alabama (CTR) site using a high-resolution time-of-flight chemical ion mass spectrometer (HR-ToF-CIMS) coupled with a filter inlet for gases and aerosols (FIGAERO) and a two-dimensional gas chromatography time-of-flight mass spectrometer (GCxGC-ToF-MS) (Zhang et al., 2018a). Observed ($T_{g,org}:T$), signifying the dry phase state, were estimated using Shiraiwa et al's $T_g$ parameterization from $O:C$ and $M$ and collected at the CTR site (Zhang et al., 2018a). The dry $T_{g,org}:T$ was estimated from OA observations given the absence of ALW in measurements and the Shiraiwa parameterization was used due to the lack of $C^0$ values for OA at this site (Zhang et al., 2018a). IEPOX-SOA measurements were taken from the CTR and Look Rock, Tennessee (LRK) 2013 SOAS field campaign sites (Budisulistiorini et al., 2017; Shiraiwa et al., 2017; Zhang et al., 2018a). IEPOX-SOA was measured at the CTR site using an aerosol mass spectrometer and positive matrix factorization (Hu et al., 2016; Ulbrich et al., 2009). IEPOX-SOA at the LRK site was measured using gas chromatography/electron ionization mass spectrometry (GC/EI-MS) and ultra-performance liquid chromatography/diode array detection-electrospray ionization-high-resolution quadrupole time-of-flight mass spectrometry (UPLC/DAD-ESI-HR-QTOFMS) with resolved AIETET and AIEOS measurements (Budisulistiorini et al., 2017).

## 3 Results

### 3.1 Phase separation frequency across space and altitude

The frequency of aerosol phase separation predicted at different model layers across the U.S. is shown in Figure 2. At the surface (Fig. 2a), phase separation occurs 90-100% of the time in the southeastern U.S. and western U.S. which can be attributed to lower $O:C_{avg}$ (ranging from 0.4-0.6) in the Southeast and lower RH (ranging between 10-40%) in the West. Over the oceans and Great Lakes, phase separation frequency decreases due to both high RH (≥80%) and high O:C (≥0.7). Phase separation frequencies in layer 18 (representing the lower troposphere) (Fig. 2b) decrease over the eastern U.S. largely corresponding to increases in $O:C_{avg}$ (by ~0.1 on average) where RH increases on average by ~5%. Phase separation continues to increase in layers 28 (representing the upper troposphere) (Fig. 2c) and 35 (representing the lower stratosphere) (Fig. 2d) corresponding with continued decreases in RH with altitude.

https://doi.org/10.5194/egusphere-2025-2253
Preprint. Discussion started: 5 August 2025
© Author(s) 2025. CC BY 4.0 License.

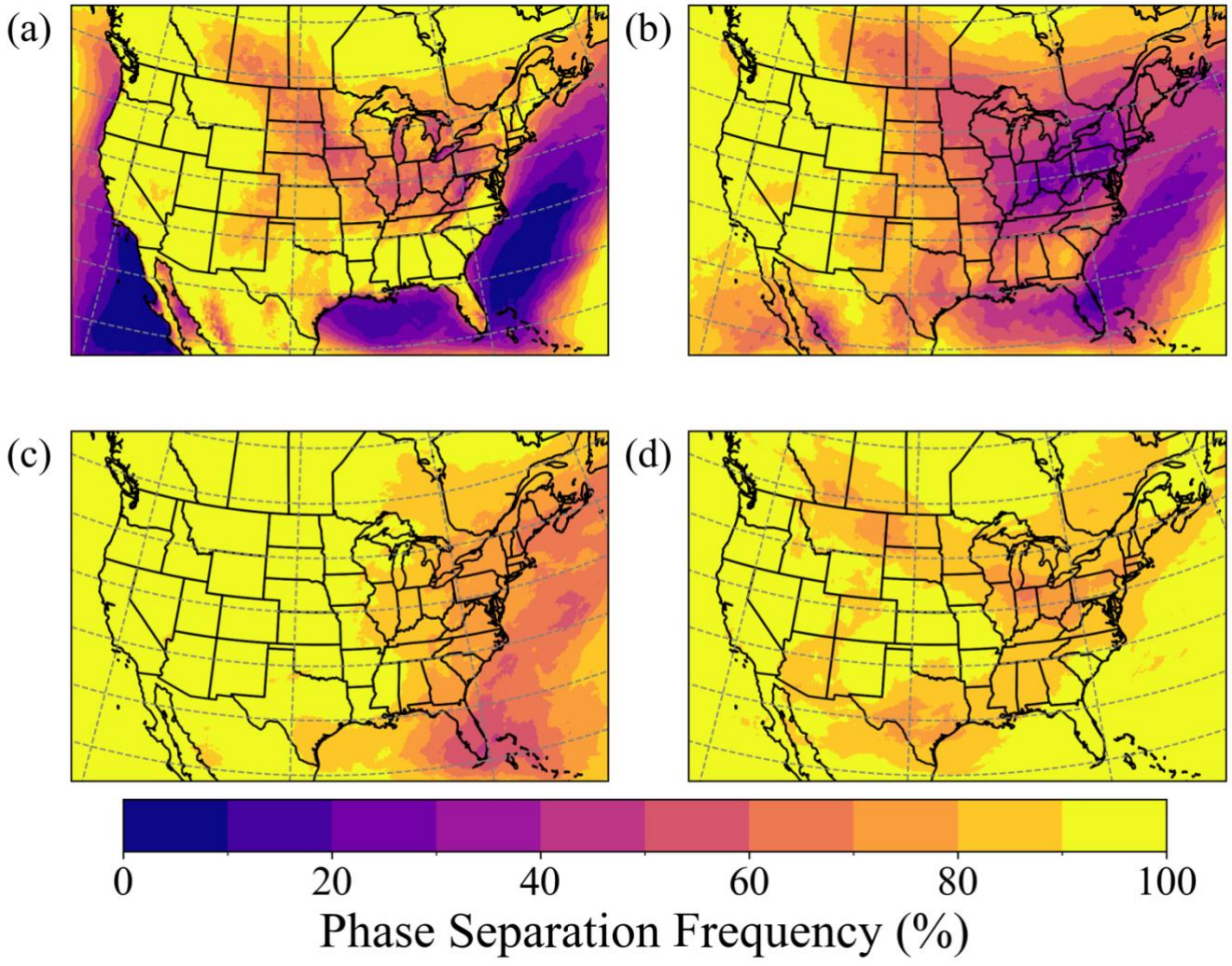


**Figure 2.** Frequency of modelled aerosol phase separation for the SOAS 2013 Field Campaign episode (June 1st – July 15, 2013) at layer 1 (surface layer (a)), layer 18 (corresponding to ~1.8km (b)), layer 28 (corresponding to ~8km (c)), and layer 35 (corresponding to ~17km (d)) across hourly model estimations.

The aggregated phase separation frequency across the first layer in this work was estimated to be 71.4 % which compares well with 68.5% predicted in Schmedding et al. (2020) though slightly higher (Schmedding et al., 2020). This difference can be attributed to a slightly lower $O{:}C_{avg}$ with the SAPRC07tic_ae7 mechanism compared to the CB6R3 mechanism in (Schmedding et al., 2020). At the CTR SOAS site, the phase separation frequency is ~97.9%, significantly higher than that reported in Schmedding et al. (2020) (i.e., 65.4%) and in Pye et al. (2017) (i.e., 79.1%). This suggest that phase separation predicted in this study at the CTR SOAS site may represent an upper bound (Pye et al., 2017; Schmedding et al., 2020).

https://doi.org/10.5194/egusphere-2025-2253
Preprint. Discussion started: 5 August 2025
© Author(s) 2025. CC BY 4.0 License.

### 3.2 Phase state of the organic coating across space and altitude

Following criteria used in Schmedding et al. (2020), a liquid phase organic coating is predicted when $T_g(w_{org}): T < 0.8$ or $T_{g,org}: T < 0.8$, a semi-solid phase organic coating when $0.8 \leq T_g(w_{org}): T < 1$ or $0.8 \leq T_{g,org}: T < 1$, and a solid phase organic coating when $T_g(w_{org}): T \geq 1$ or $T_{g,org}: T \geq 1$ (Schmedding et al., 2020). The frequency of time that the organic coating of an aerosol is in a liquid phase in layer 1 (i.e., ground level, GL) across the whole modeling episode when an appreciable amount of ALW is present in the organic coating (when $w_s > 0.1$) and when $w_s \leq 0.1$, corresponding to $T_g(w_{org}): T$ and $T_{g,org}: T$, is shown in Figure 3. The southeast U.S. has the highest frequency of a liquid phase organic coatings in all three parameterizations when ALW is present in the organic coating across all model simulations with a distinct transition going from east to west (Fig. 3 a-c). The southeast is known to experience hot and humid summers with both increased temperatures and increased ALW expected to plasticize the organic coating.

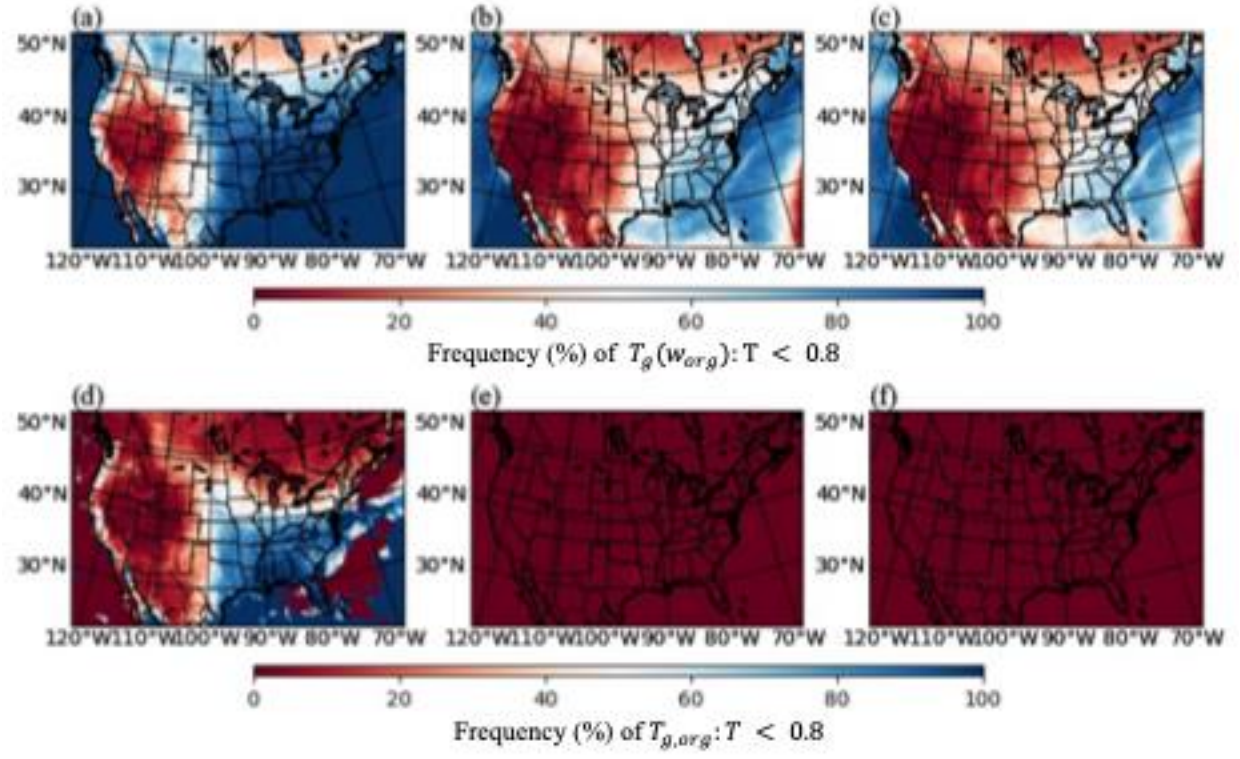


**Figure 3.** Frequency that the organic coating is in the liquid phase state for the (a & d) Shiraiwa, (b & e) Zhang and (c & f) Li parameterizations when $\boldsymbol{w_s > 0.1}$ in the organic coating (a-c) and when $\boldsymbol{w_s \leq 0.1}$ in the organic coating (d-f) across hourly model estimates.

https://doi.org/10.5194/egusphere-2025-2253
Preprint. Discussion started: 5 August 2025
© Author(s) 2025. CC BY 4.0 License.

When $w_s > 0.1$ the Li and Zhang simulations predicted a higher frequency of semi-solid and solid organic coatings across the U.S in comparison to the Shiraiwa simulation with the liquid-to-solid transition zone moving further west (Fig. 3 a-c). Zhang et al. (2018b) found that IEPOX uptake is phase state limited ~40% of the time in the Southeast U.S (Zhang et al., 2018b) which agrees qualitatively with the Zhang and Li simulations. The western U.S. shows distinctly less frequent liquid organic coatings (when $w_s > 0.1$) for all simulations (Fig. 3 a-c) corresponding with decreased RH.

The $T_g(w_{org}):T$ of the organic coating also increases with altitude, as shown in Figure 4. In the surface layer of the model (Layer 1; @GL), across all grid cells and hourly timesteps, the Shiraiwa simulation predicts the highest frequency of the liquid phase state, in agreement with Fig. 3a. The Zhang and Li simulations show a slightly lower liquid phase state frequency. In layer 18, the Shiraiwa simulation also predicts the highest frequency of the liquid phase state (~50% of the time) in comparison to the Zhang and Li simulations. While the phase state of the organic coating at the surface and lower troposphere (layer 18) are important for heterogeneous chemistry, the phase state of the organic coating in the upper troposphere (layer 28) and lower stratosphere (layer 35) are important for cirrus cloud formation (Berkemeier et al., 2014; Murray et al., 2010; Wolf et al., 2020). In all simulations at layers 28 and 35, the phase state of the organic coating is mostly semi-solid to solid given lower RH and lower $T$ at higher altitudes. This phase state can potentially provide a surface for heterogeneous ice cloud nucleation via deposition (Berkemeier et al., 2014; Murray et al., 2010; Wolf et al., 2020).

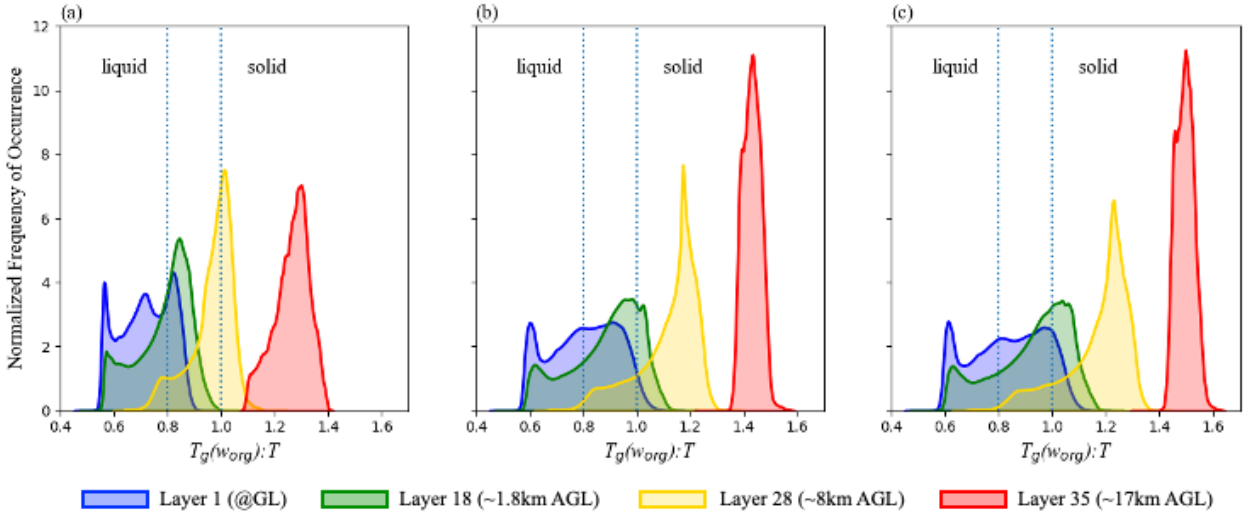


**Figure 4.** The normalized frequency of occurrence of organic coating phase states (when $\boldsymbol{w_s > 0.1}$; $(\boldsymbol{T_g(w_{org}):T})$) across the surface spatial domain and for the entire simulation period (hourly model estimations) for modeled layers 1 (blue, GL = ground level), 18 (green, 1.8 km AGL = above ground level), 28 (yellow, 8 km AGL), and 35 (red, 17 km AGL). Shown are the estimates using the Shiraiwa (a), Zhang (b), and Li (c) simulations. Dotted blue lines representing the bounds for the three different phase states: liquid, semi-solid, and solid.

https://doi.org/10.5194/egusphere-2025-2253
Preprint. Discussion started: 5 August 2025
© Author(s) 2025. CC BY 4.0 License.

Recent studies have indicated that ALW has the most significant effect on aerosol phase state (Li et al., 2021; Rasool et al., 2021). The influence that ALW in the organic coating has on phase state is demonstrated by the comparison to the frequency of the liquid phase state when $w_s \leq 0.1$ (Fig 3. d-f). While all simulations predict some liquid organic coatings in the Eastern U.S. when $w_s > 0.1$ (Fig. 3 a-c), both the Zhang and Li parameterizations almost never predict a liquid phase organic coating at $w_s \leq 0.1$ (Fig 3. d-f). However, the frequency of the liquid phase state for the Shiraiwa model run is still $\geq 80\%$ in the Southeastern U.S., whereas the Li and Zhang simulations are 90-100% in the semi-solid phase state. While ALW is a significant modulator of the organic coating's phase state, the composition and $T_g$ equation used can also impact the phase state.

### 3.3 The influence of $T_g$ equations on organic coating phase state

Phase state differences across the three model parameterizations are partially due to differences in individual OA component's $T_g$ values. The $T_g$ values predicted by the Shiraiwa equation for each OA species along with differences between the Shiraiwa, Zhang and Li equations are shown in Table 2. The largest differences in $T_g$ value where those of the isoprene organic nitrates (AISOPNN) between the Shiraiwa and Zhang equations (Table 2) differing by 143K. The Shiraiwa equation predicts a solid $T_g$ at normal surface temperatures, while the Zhang parameterization allows prediction of a semi-solid or liquid phase. Since the Zhang equation takes into consideration ambient temperatures in predicting $T_g$, the comparison was made at 298K. AISOPNN has a higher $M$ and $O{:}C$, which would increase its $T_g$, however a higher $C^0$ relative to most OA species, which would decrease its $T_g$, and therefore would contribute to these differences.

**Table 2.** Glass transition temperatures ($\boldsymbol{T_g}$) predicted for each OA species in the SAPRC07tic_ae7i mechanism for the Shiraiwa equation and percent differences between the Zhang and Shiraiwa equations, the Li and Shiraiwa equations, and between the Zhang and Li equations.

https://doi.org/10.5194/egusphere-2025-2253
Preprint. Discussion started: 5 August 2025
© Author(s) 2025. CC BY 4.0 License.

| CMAQ Species | Species Description | Molar Mass (g/mol) | $\log_{10}(C^0)$ | O:C | Source | Shiraiwa $T_g$ (K) | Differences (K) (Zhang @298K - Shiraiwa) | Differences (K) (Li - Shiraiwa) | Differences (K) (Li - Zhang @298K) |
|---|---|---|---|---|---|---|---|---|---|
| AISOPNN | isoprene organic nitrates | 226 | 0.94 | 2.11 | biog | 391 | -143 | -111 | 33 |
| AIMOS | methacrolein epoxide derived organosulfate | 200 | -1.25 | 2.40 | biog | 408 | -119 | -108 | 11 |
| AIEOS | IEPOX-derived methyltetrol sulfate | 216 | -2.40 | 1.95 | biog | 376 | -68 | -64 | 4 |
| AIVPO1 | IV primary organic compounds | 266 | 3.00 | 0.00 | anth | 260 | -60 | -23 | 37 |
| AOLGA | oligomer products of anthropogenic SOA compounds | 206 | 0.88 | 1.07 | anth | 303 | -55 | -25 | 30 |
| ASQT | SV SOA from sesquiterpenes | 273 | 1.40 | 0.28 | biog | 282 | -43 | -15 | 28 |
| AOLGB | oligomer products of biogenic SOA compounds | 248 | 0.42 | 0.75 | biog | 300 | -41 | -17 | 24 |
| AMTNO3 | SV organic nitrates from monoterpene oxidation | 231 | 1.08 | 0.59 | biog | 280 | -35 | -7 | 29 |
| ASVPO3 | SV primary organic compounds | 253 | 2.00 | 0.03 | anth | 254 | -30 | 1 | 31 |
| AAVB4 | SV organic particulate matter from oxidation of anthropogenic VOCs | 158 | 2.00 | 0.67 | anth | 236 | -16 | 23 | 40 |
| AAVB3 | SV organic particulate matter from oxidation of anthropogenic VOCs | 169 | 1.00 | 0.81 | anth | 257 | -14 | 18 | 32 |
| AISO1 | SV SOA product from isoprene | 132 | 2.06 | 0.83 | biog | 229 | -13 | 30 | 43 |
| AIMGA | 2-methylglyceric acid | 120 | 1.34 | 1.07 | biog | 243 | -11 | 28 | 39 |
| AAVB1 | LV organic particulate matter from oxidation of anthropogenic VOCs | 198 | -2.00 | 1.24 | anth | 313 | -11 | 0 | 12 |
| AAVB2 | SV organic particulate matter from oxidation of anthropogenic VOCs | 179 | 0.00 | 0.88 | anth | 271 | -6 | 18 | 25 |
| AMT6 | SV particulate matter from monoterpene photooxidation | 168 | 3.00 | 0.15 | biog | 198 | -3 | 41 | 43 |
| ASVPO2 | SV primary organic compounds | 241 | 1.00 | 0.07 | anth | 249 | -2 | 24 | 26 |
| AMTHYD | organic pseudo-hydrolysis accretion product from monoterpene organic | 186 | 1.72 | 0.30 | biog | 226 | 2 | 36 | 34 |
| AMT1 | LV particulate matter from monoterpene photooxidation | 300 | -2.00 | 0.37 | biog | 299 | 5 | 19 | 14 |
| AMT5 | SV particulate matter from monoterpene photooxidation | 170 | 2.00 | 0.30 | biog | 213 | 8 | 44 | 37 |
| AMT4 | SV particulate matter from monoterpene photooxidation | 184 | 1.00 | 0.30 | biog | 224 | 20 | 49 | 29 |
| ADIM | 2-methyltetrol dimer | 248 | -3.16 | 0.72 | biog | 299 | 22 | 32 | 11 |
| ASVPO1 | SV primary organic compounds | 230 | 0.00 | 0.12 | anth | 245 | 22 | 44 | 22 |
| AMT3 | SV particulate matter from monoterpene photooxidation | 186 | 0.00 | 0.44 | biog | 238 | 27 | 51 | 24 |
| AIETET | 2-methyltetrol | 136 | -0.33 | 0.88 | biog | 238 | 30 | 55 | 25 |
| AISO2 | SV SOA product from isoprene | 133 | -0.21 | 0.85 | biog | 233 | 33 | 59 | 26 |
| ASVOO3 | SV oxidized combustion organic products | 134 | 2.00 | 0.35 | anth | 184 | 34 | 73 | 39 |
| AMT2 | LV particulate matter from monoterpene photooxidation | 200 | -1.00 | 0.37 | biog | 243 | 42 | 62 | 20 |
| ALVPO1 | LV primary organic compounds | 218 | -1.00 | 0.18 | anth | 241 | 44 | 64 | 20 |
| ASVOO2 | SV oxidized combustion organic products | 135 | 1.00 | 0.45 | anth | 195 | 46 | 78 | 33 |
| ASVOO1 | SV oxidized combustion organic products | 135 | 0.00 | 0.57 | anth | 207 | 55 | 82 | 27 |
| AORGC | cloud-formed SOA | 177 | -2.52 | 0.67 | biog | 251 | 58 | 73 | 15 |
| ALVOO2 | LV oxidized combustion organic compounds | 136 | -1.00 | 0.71 | anth | 222 | 59 | 81 | 22 |
| ALVOO1 | LV oxidized combustion organic compounds | 136 | -2.00 | 0.88 | anth | 238 | 60 | 77 | 17 |
| AGLY | glyoxal / methylglyoxal SOA | 66.4 | -1.34 | 0.77 | biog | 160 | 70 | 90 | 21 |
| APCSO | potential combustion SOA | 170 | -5.00 | 0.67 | anth | 245 | 96 | 108 | 12 |

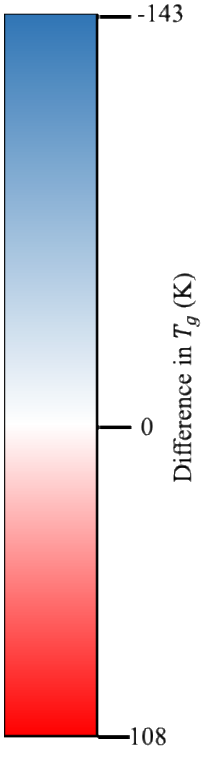


For most species, the Zhang and Li equations predict a higher $T_g$ than the Shiraiwa equation, particularly potential combustion SOA (APCSO) and glyoxal- and methylglyoxal-derived aerosol (AGLY). The $M$ of APCSO is 170 g/mol and the $O{:}C$ is 0.67, however it has the lowest $C^0$ of all the OA species (0.00001 μg/m$^3$) which would be the main influence on predicting $T_g$ in the Zhang and Li equations. With the Shiraiwa equation, AGLY has a $T_g$ of 160K (meaning the ambient temperature would need to be 200K for it to be in a semi-solid phase and 160K for it to be in a solid phase state) and therefore at normal surface temperatures for this modeling episode and domain, AGLY would always be in a liquid phase state. It should be noted that the $M$ used for AGLY is 66.4 g/mol, while the surrogate species used to estimate the $C^0$ for AGLY is ammonium oxalate – a

https://doi.org/10.5194/egusphere-2025-2253
Preprint. Discussion started: 5 August 2025
© Author(s) 2025. CC BY 4.0 License.

common particle-phase product of both glyoxal and methylglyoxal - which has a published low vapor pressure of 1.7 x $10^{-6}$ Pa (Paciga et al., 2014). If the $M$ of ammonium oxalate's true molar mass (124 g/mol) were to be used instead, the $T_g$ predicted for AGLY in the Shiraiwa parameterization would increase to 216K, which could increase the $T_g(w_{org})$ or the $T_{g,org}$ for this simulation.

As shown in Supplemental Figure 2, the model predicts an aerosol composition mainly influenced by CMAQ biogenic species in the Southeastern U.S. and the Western U.S. Supplemental Figure 3a shows that the biogenic species with the highest contribution to biogenic aerosol mass in these regions are monoterpene-derived hydration products (AMTHYD), and low-volatility monoterpene SOA species (AMT1 and AMT2). As shown in Table 2, while the $T_g$ predicted by the Shiraiwa and Zhang equations agree within 2K for AMTHYD, the Li equation predicts a $T_g$ 34-36K higher. Nonetheless for this modeling episode and domain, $T_g$'s of 226-262K would still likely indicate a liquid phase state at the surface. Differences in $T_g$ for AMT1 may impose more differences in phase state given the range in predicted $T_g$ is 299-318K and the $T_g$ for AMT2 ranges from 243K-305K.

In the northern Midwest, the leading contribution to aerosol mass were anthropogenic species (Fig. S2), and the leading anthropogenic species were semi-volatile oxidized combustion organic products (ASVOO1) and low-volatility oxidized combustion organic products (ALVOO2) (Fig. S3a&b). For ASVOO1, $T_g$ ranges from 207K-289K, while for ALVOO2, $T_g$ ranges from 222K-303K (Table 2). These species and their range of $T_g$ is likely the cause for the differences in the liquid-to-solid transition in the northern Midwest (Fig. 3a-c) across all model simulations.

### 3.4 Comparison of modelled $T_{g,org}:T$ to derived observations

Figure 5 shows the 2013 SOAS CTR ground site estimated $T_{g,org}:T$ diurnal profile and the predicted $T_{g,org}:T$ (when $w_s \leq 0.1$) diurnal profiles for each parameterization at that grid cell, with vertical fliers representing one standard deviation. It should be noted that observations did not account for ALW, and thus, it would be inappropriate to compare them with $T_g(w_{org}):T$. The Shiraiwa parameterization predicted the lowest $T_{g,org}:T$ at the CTR site. The Zhang and the Li predictions of $T_{g,org}:T$ were higher with similar diurnal profiles. Modeled $O:C_{avg}$ are biased low, having a normalized mean bias (NMB) of ~ -0.25, compared to observed $O:C_{avg}$ at the SOAS CTR site, and are lower than $O:C_{avg}$ predicted in Schmedding et al. (Schmedding et al., 2020; Zhang et al., 2018a). While this may influence model-measurement comparisons, $O:C$ ratios were found to have a minor influence of phase state in comparison to OA, $M$, and $w_s$ (Koop et al., 2011; Li et al., 2020; Shiraiwa et al., 2017). As noted previously (Sect. 2.4), there remains a disconnect between modeled $M$ and modeled $C^0$ in CMAQ which

https://doi.org/10.5194/egusphere-2025-2253
Preprint. Discussion started: 5 August 2025
© Author(s) 2025. CC BY 4.0 License.

could explain why the Shiraiwa predicted $T_{g,org}:T$ were biased low and lower than the other two parametrizations. Estimations of measured $T_{g,org}:T$ at the CTR SOAS site (Fig. 5) may also be biased low given that $C^0$ values were not measured.

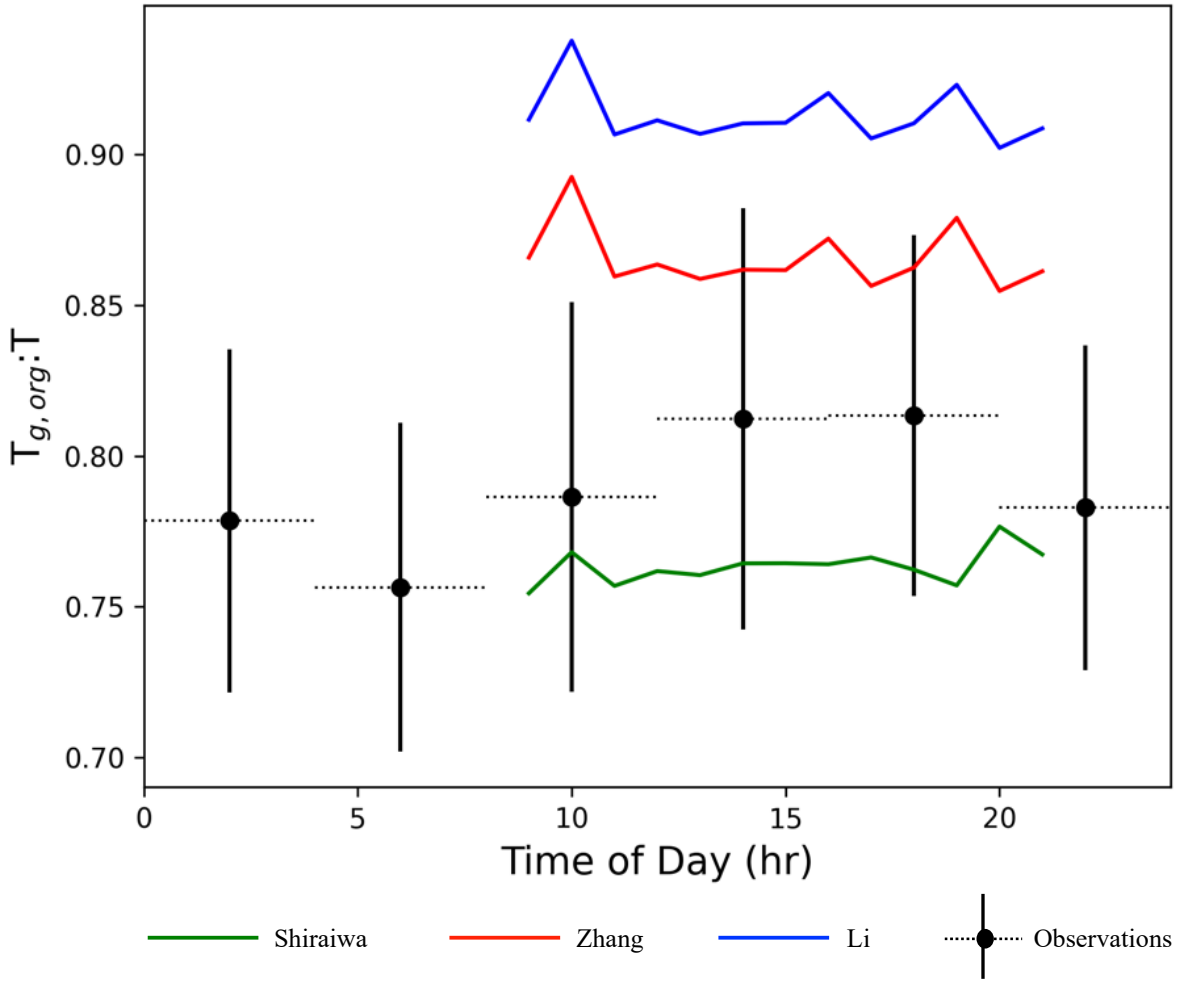


**Figure 5.** Diurnal comparisons of model predicted and observed $\boldsymbol{T_{g,org}:T}$ for the Shiraiwa, Zhang and Li model simulations at the CTR SOAS site for June 1st 2013 – July 15th 2013. Flyers on observations represent 1 standard deviation.

### 3.5 Impacts on IEPOX-SOA Modeled Formation

Episode-averaged IEPOX reactive uptake coefficients, $\gamma_{IEPOX}$, were compared across simulations (Figure 6). The episode-averaged base model predictions of $\gamma_{IEPOX}$ ranged from $10^{-6} - 10^{-3}$, with the average value at the LRK SOAS site being $6.21 \times 10^{-4}$, which is in agreement with episode-averaged value from Budisulistiorini et al. (i.e. $3.2 \times 10^{-4}$), though slightly higher (Budisulistiorini et al., 2017). The diffusional hindrance to heterogeneous IEPOX reactive uptake due to existing

https://doi.org/10.5194/egusphere-2025-2253
Preprint. Discussion started: 5 August 2025
© Author(s) 2025. CC BY 4.0 License.

viscous organic coatings had the largest impact in the western part of the U.S., reducing $\gamma_{IEPOX}$ by 80-99% (Fig. 6). In most of the western U.S. the abundance of IEPOX is limited (Fig. S1), with the exception of coastal Northern California where these decreases can potentially impact model performance in estimating IEPOX-SOA and total OA (Fig. 6). IEPOX concentrations are also appreciable in parts of Canada (Fig. S1) where $\gamma_{IEPOX}$ reductions can be $> 0.001$ (representing up to a 99.99% reduction). In the Southeast U.S. (where IEPOX concentrations peak (Fig. S1)) predicted reductions in $\gamma_{IEPOX}$ range from 20-80% depending on the phase state simulation used. At the LRK SOAS site, $\gamma_{IEPOX}$ were reduced to values ranging from $3.5 \times 10^{-4}$ to $4.84 \times 10^{-4}$ and are in closer agreement to values in Budisulistiorini et al. (Budisulistiorini et al., 2017). The $D_{org,eff}$ across all simulations ranges between $10^{-12} - 10^{-13}$ m$^2$/s and are in agreement with box modeling of resistance to IEPOX reactive uptake shown in (Chen et al., 2024). Increases in $\gamma_{IEPOX}$ occur over the oceans and are up to ~0.0001 and account for up to ~7% percent increase and these bounds can be considered a consequence of numerical noise along with decreases of the same magnitude. The phase state and phase separation model run-times are ~5% slower in all of the sensitivity runs compared with the base.

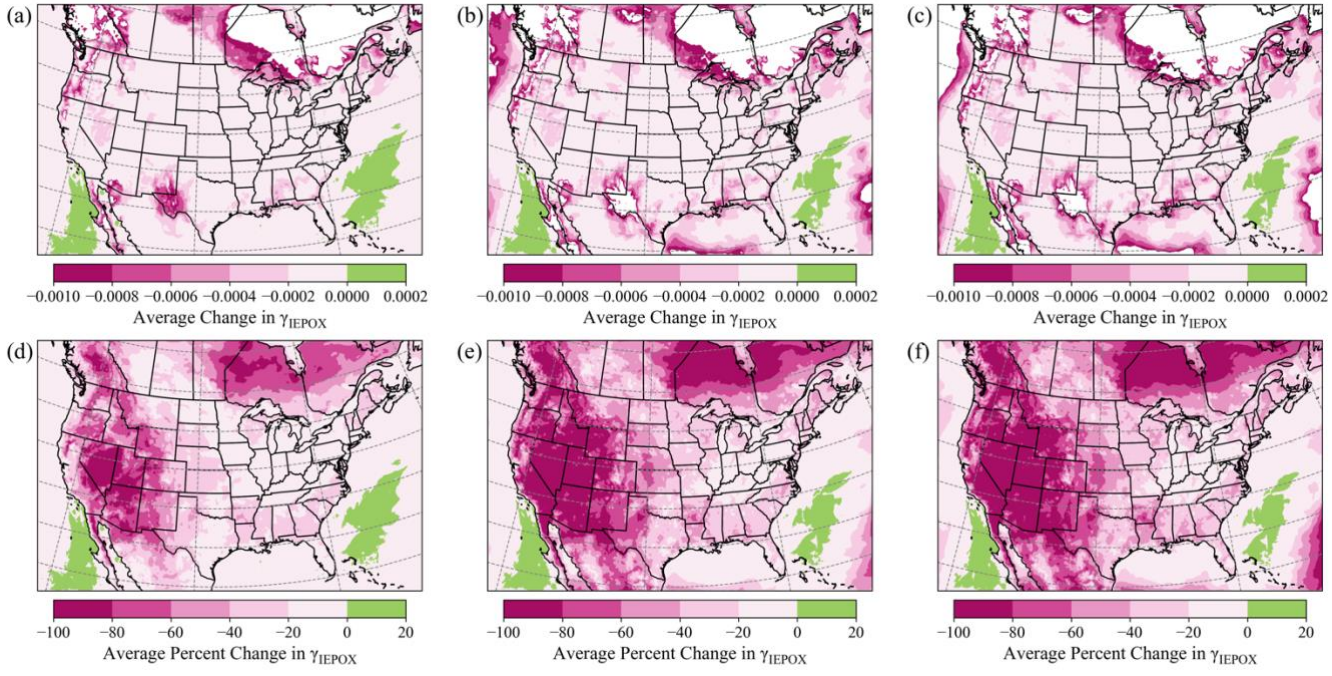


**Figure 6.** Average difference in IEPOX-SOA reactive uptake coefficients ($\boldsymbol{\gamma_{IEPOX}}$) from the base (no organic coatings resistor term) simulation compared to $\boldsymbol{\gamma_{IEPOX}}$ predicted by Shiraiwa (a), Zhang (b), and Li (c) model simulations. Average percent changes in $\boldsymbol{\gamma_{IEPOX}}$ from the base model simulation compared to $\boldsymbol{\gamma_{IEPOX}}$ predicted by Shiraiwa (d), Zhang (e), and Li (f) model simulations. White spaces represent areas where the average differences are below -0.001.

https://doi.org/10.5194/egusphere-2025-2253
Preprint. Discussion started: 5 August 2025
© Author(s) 2025. CC BY 4.0 License.

With the implementation of phase separation, water diffusing from the inorganic core to the organic coating was not considered and therefore inorganic ion aqueous concentrations were not directly impacted by phase separation. This is important to note given that increasing $k_{particle}$ from $10^{-3}$/s to $10^{-2}$/s results in an increase in $\gamma_{IEPOX}$ by ~740% of magnitude (assuming an organic coating radius of 50 nm and $T = 298K$) (SI Eq. 3). An increase in $D_{org,eff}$ from $10^{-13}$ m$^2$/s to $10^{-12}$ m$^2$/s results in an increase in $\gamma_{IEPOX}$ by ~0.02% (assuming an organic coating radius of 50 nm and $T = 298K$) (SI Eq. 3).

Total predicted IEPOX-SOA concentrations were compared between each parameterization (including base CMAQv5.3) and the observations obtained at the CTR SOAS site (Hu et al., 2016) shown in Figure 7a. The base CMAQ run had the best model performance in simulating total IEPOX-SOA, yet still underpredicted observations, with an NMB of -0.37. Model performance in predicting IEPOX-SOA concentrations worsened when including phase separation and phase state with NMB's of -0.48, -0.53, and -0.56 for the Shiraiwa, Zhang, and Li parameterizations.

https://doi.org/10.5194/egusphere-2025-2253
Preprint. Discussion started: 5 August 2025
© Author(s) 2025. CC BY 4.0 License.

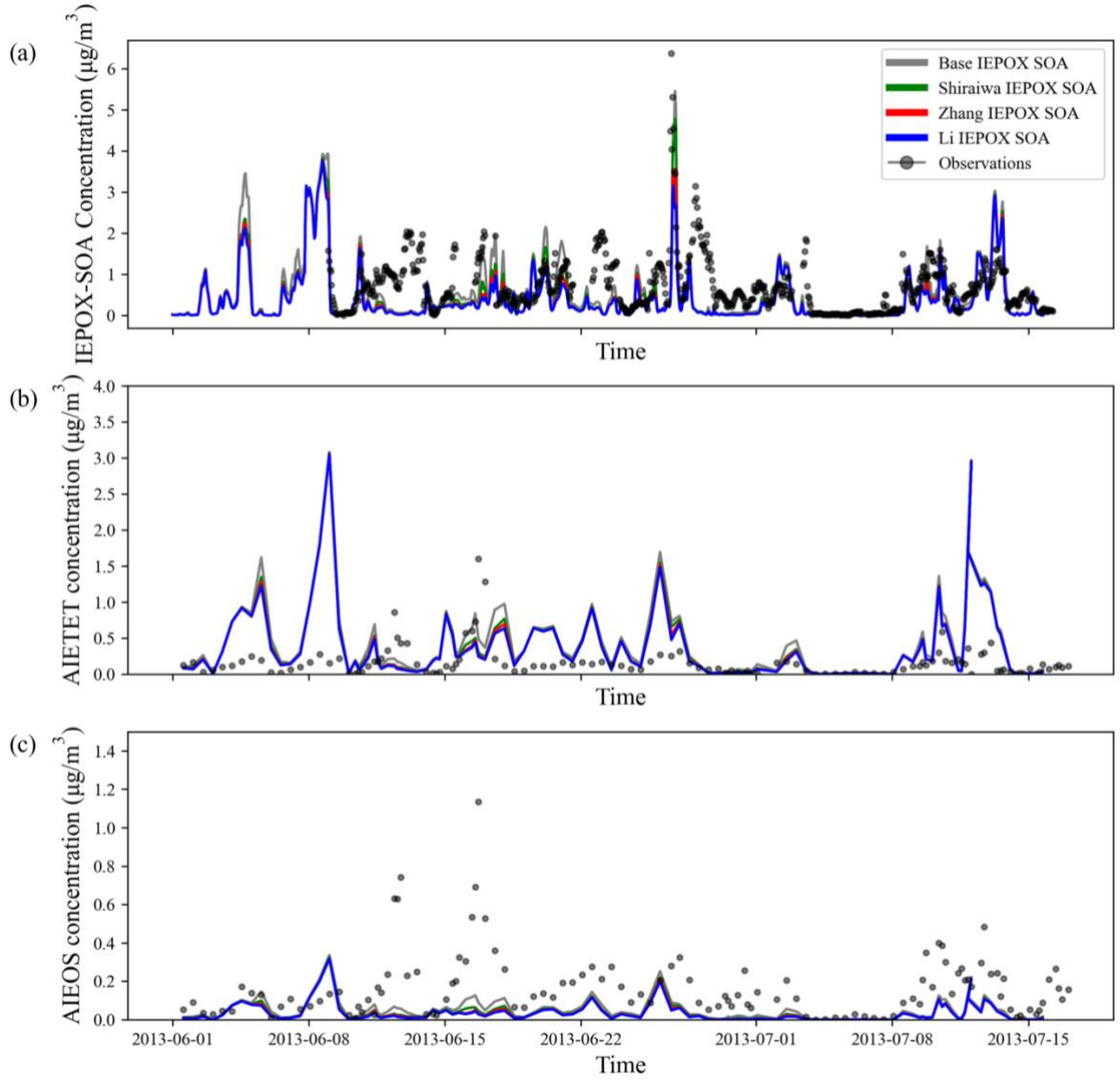


**Figure 7.** Observational and predicted concentrations of (a) total IEPOX-SOA at CTR and (b) AIETET and (c) AIEOS at the LRK SOAS site for June 1st – July 15th, 2013. Predicted concentrations are shown for base CMAQ (grey), Shiraiwa (green), Zhang (red), and Li (blue) model simulations.

Observations of specific IEPOX-derived SOA tracers at LRK, including 2-methyltetrols (AIETET) and IEPOX organosulfates (AIEOS), were compared with corresponding CMAQ species concentrations (Fig. 7b-c) (Budisulistiorini et al., 2015a). The LRK site is situated in the Great Smoky Mountains, where the altitude (~ 800 m above sea level) can affect both temperature and RH. CMAQ predicts temperatures ranging from 290K-302K at this site for the duration of the SOAS campaign, with

https://doi.org/10.5194/egusphere-2025-2253
Preprint. Discussion started: 5 August 2025
© Author(s) 2025. CC BY 4.0 License.

predicted $w_s$ values ranging from 0.1-0.6. Differences in IEPOX-SOA predictions across model runs at the LRK site coincide with both low temperatures and low $w_s$. AIETET is overpredicted most of the time for all parameterizations (including the base run), with the base run having a NMB of 1.54. For the model runs accounting for phase separation and phase state, the bias improves with NMBs of 1.26, 1.19, and 1.14 for the Shiraiwa, Zhang, and Li parameterizations, respectively. It is important to note the recent studies have suggested that AIETET can off-gas (D'Ambro et al., 2019; Riedel et al., 2015); however, heterogeneous oxidation experiments of IEPOX-SOA have also suggested aged IEPOX-SOA (which produces more functionalized oligomer species) may limit this off-gassing (Armstrong et al., 2022; Hu et al., 2016). The base CMAQ run underpredicts AIEOS concentrations with a NMB of -0.66. All parameterizations accounting for phase separation and phase state underpredict AIEOS concentrations further with NMBs of -0.73, -0.75, and -0.76 for the Shiraiwa, Zhang, and Li parameterizations, respectively, throughout the modeled episode of the SOAS campaign. These underpredictions of AIEOS coincide with underpredictions in sulfate concentrations (Figure S4), which may decrease the branching of IEPOX-SOA towards AIEOS. The highest IEPOX-SOA is coincided with the highest inorganic sulfur concentrations (Chen et al., 2021), and the formation of IEPOX-derived organosulfates depends partially on high acidity and availability of nucleophiles ($H_2O$ and sulfate) (Brüggemann et al., 2020; Piletic et al., 2013). Updating sulfate formation mechanisms to include heterogeneous sulfur chemistry in ALW (Farrell et al., 2024), along with increasing the AIEOS branching fraction, may help resolve this bias for all model runs (including the Base) (Budisulistiorini et al., 2017; Chen et al., 2024). Lastly, there is uncertainty in the how to model branching ratios between AIETET and AIEOS arising from the reported variability of sulfate ion activity (Petters et al., 2021). Organosulfates have been recently predicted and demonstrated to be surface active species, and thus, their incorporation into total ion activity could change previous branching ratio parameterizations (Hyttinen et al., 2020; Olson et al., 2019; Riva et al., 2019).

## 4 Discussion

### 4.1 Modulators of organic coating phase state

Model predictions show that both the $w_s$ and the choice in $T_g$ parameterization impact the phase state of the organic coating on phase-separated aerosols. Previous studies have shown the influence of ALW on the phase state of organic aerosols (DeRieux et al., 2018; Rasool et al., 2021). This represents the first study to also compare the impacts of different $T_g$ parameterizations on phase state in a chemical transport air quality model, providing insight into ranges of organic coating phase states that can occur. To disentangle the effects of $T_g$ parameterizations and the effect of ALW, the phase state of the organic coating was analyzed when $w_s \leq 0.1$ (Fig. 3 d-f). When $w_s \leq 0.1$ the Shiraiwa run still predicted a liquid phase state in the Southeast U.S., whereas the Zhang and Li simulations predicted a semi-solid organic coating. This difference in predictions can partially be explained by inconsistencies in CMAQ species properties and each $T_g$ parameterization leveraging different species properties (Table 1). For example, in the case of AGLY, the species molecular weight implies a much smaller

https://doi.org/10.5194/egusphere-2025-2253
Preprint. Discussion started: 5 August 2025
© Author(s) 2025. CC BY 4.0 License.

compound than the volatility ($C^0$) suggests. Two $T_g$ parameterizations use volatility while the other relies solely on $M$ and $O{:}C$. As a result, the AGLY estimated $T_g$ vary by a factor of 2 across the different methods. With the updates to $C^0$ in this work, the molar masses were not updated to reflect the proxy species used and may underpredict the $T_g$ for important species such as AGLY (Fig. S3). Species that did not require updates to $C^0$ nor $O{:}C$ still had wide ranges of predicted $T_g$ between parameterizations, particularly species that are leading contributors to OA mass (AMT1, AMT2, ASVOO1, and ALVOO2) (Fig. S3).

The methods used to derive $T_g$ parameterizations also had an impact on predicted total $T_{g,org}{:}T$. When $w_s \leq 0.1$, the Li and Zhang model simulations almost never predicted a liquid organic coating (Fig. 3d-f), and rather largely predicted a semi-solid phase state in the eastern U.S. and a solid phase state in the western U.S. When compared with derived simulations of $T_{g,org}{:}T$ (Fig. 5), predictions from the Zhang and Li parameterizations were also more viscous than that predicted in the Shiraiwa parameterization. In comparison to the Shiraiwa $T_g$ equation, the Zhang and Li $T_g$ parameterizations were fit with the inclusion of much lower-volatility OA, although not biased in that direction, and therefore may lead to a more informed estimate of phase state. In fitting $T_g$ equations, the derivations in $C^0$ between the Zhang and Li parameterizations differed with the potential to cause differences in phase state predictions (Li et al., 2020; Zhang et al., 2019b). In the Zhang parameterization, 13 OA $T_g$ values were measured (Zhang et al., 2019b), and the $p_0$ values were sourced from publications or the EVAPORATION model (Compernolle et al., 2011). In the Li parameterization, a similar process was followed in first searching the literature for established $p_0$, however, due to the lack of observed $T_g$ values of some sulfur-containing compounds, $T_g$ values for CHOS compounds (~ 35 % compounds in the training dataset) were estimated based on the Boyer-Kauzmann rule (Li et al., 2020). With using the Boyer-Kauzmann rule, melting temperatures were estimated using EPI Suite along with vapor pressures also estimated using EPI Suite (EPA, 2012; Li et al., 2020). In comparison to other structural activity relationship models, EVAPORATION predicts higher volatilities than both OPERA and EPI Suite (Mansouri et al., 2018). In addition, EPI Suite can predict higher melting temperatures than OPERA (Mansouri et al., 2018). Associating a $T_g$ with a higher volatility has the potential to lower $T_g$ and to predict a less viscous phase state, and associating a higher melting temperature with $T_g$ has the potential to predict a more viscous phase state. Ultimately, model-measurement $T_{g,org}{:}T$ performance is underpowered in this study and warrants the need for future field measurements of aerosol phase state.

### 4.2 Impacts on IEPOX reactive uptake

Across all simulations that considered the effect of phase separation and diffusivity limitations, $\gamma_{IEPOX}$ was reduced in comparison to the base simulation and to different degrees based on the aggregated phase state of the organic coating predicted (Fig. 6). These reductions resulted in furthering the negative bias in predicting total IEPOX-SOA and IEPOX organosulfates

https://doi.org/10.5194/egusphere-2025-2253
Preprint. Discussion started: 5 August 2025
© Author(s) 2025. CC BY 4.0 License.

(AIEOS) (Fig. 7a & c); however, it improved the positive bias in predicting 2-methyltetrols (AIETET). While the impacts of phase state on $D_{org,eff}$ and subsequently $\gamma_{IEPOX}$ were explored in this study, there are other parameters that $\gamma_{IEPOX}$ has been known to be more sensitive to that warrant further exploration. Without phase separation and phase state implemented, when increasing the $k_{particle}$ from 0.0001/s to 0.001/s (consistent with bounds seen in (Budisulistiorini et al., 2017), $\gamma_{IEPOX}$ increases by one order of magnitude. The AIEOS specific third-order rate constant used here (Table S3) and in previous studies (Budisulistiorini et al., 2017; Riedel et al., 2016) is slower than that determined by (Piletic et al., 2013) (based on AIEOS:AIETET from laboratory studies) (Budisulistiorini et al., 2017; Riedel et al., 2016), and may be partially responsible for the underpredictions in AIEOS and total IEPOX-SOA. As the AIEOS:AIETET ratio is considered in determining the third-order rate constant for AIEOS (Budisulistiorini et al., 2017), it has been suggested that this rate constant should be higher (Chen et al., 2024), which could work to increase $\gamma_{IEPOX}$ to a level consistent with chamber studies (D'Ambro et al., 2019). The total $k_{particle}$ for the formation of AIEOS also depends on particle acidity (Cooke et al., 2024; Gaston et al., 2014; Riedel et al., 2016; Riva et al., 2016) and particulate sulfate concentrations (Cooke et al., 2024; Jo et al., 2021; Riva et al., 2019) (Eq. S5, Table S3) (Eddingsaas et al., 2010), and an underprediction in AIEOS and subsequently IEPOX-SOA, can possibly be attributed to model underpredictions of sulfate (Fig. S4). The addition of missing heterogeneous sulfate formation pathways increased the mean bias in sulfate concentration predictions at the LRK site by ~0.2 $\mu g/m^3$ for July 2016 (Farrell et al., 2024) and could potentially help resolve model-measurement differences for AIEOS. A combination of increased particle-phase reaction rates due to increased sulfate and volatilization of 2-methytetrols could improve both the ratio of predicted 2-methyltetrols to organosulfates as well as their overall abundance in model predictions. A limitation of this study is that water did not move between the organic coating and the inorganic aqueous core (Schmedding et al., 2023), which may pose another impact on the $k_{particle}$ – increasing it or decreasing it based on dilution or concentration of acids and nucleophiles (Cooke et al., 2024; Gaston et al., 2014; Riva et al., 2016).

### 4.3 Atmospheric Implications

The inclusion of dynamic phase separation state should be further evaluated in the context of climate (Schill et al., 2013; Wagner et al., 2012) and meteorological modeling (Fard et al., 2018; Zhang et al., 2022), as well as on human health endpoint studies (Mu et al., 2018; Shrivastava et al., 2017). For all sensitivity simulations, in higher layers of the modeling grid (> 8km; i.e., model vertical layers exceeding 28$^{th}$ layer), the phase state of the outer organic coating was in either a semi-solid or solid phase state attributed to modeled RH (less than 60%) and modeled $T$ (less than 262K) (Fig. 4). The phase state (influenced by RH and temperature) of phase-separated aerosols have been shown to influence liquid water uptake to solidified inorganic cores (immersion freezing) (Berkemeier et al., 2014) and the formation of ice from water vapor on the outer organic coating (heterogeneous depositional freezing) (Murray et al., 2010). These processes have implications for the formation of cirrus clouds (Berkemeier et al., 2014; Cziczo et al., 2013; Murray et al., 2010; Wagner et al., 2012; Wolf et al., 2020). Heterogeneous

https://doi.org/10.5194/egusphere-2025-2253
Preprint. Discussion started: 5 August 2025
© Author(s) 2025. CC BY 4.0 License.

depositional freezing would be a particularly important pathway for cirrus cloud formation in the context of this work, as the mixing time of water and organic species at higher altitudes—where air-mass updrafts increase cooling rates and RH is lower—has been shown to exceed modeled time-steps for assumed thermodynamic equilibrium (Maclean et al., 2021).

The effect of phase separation on liquid cloud droplet activation is also an ongoing area of research (Davies et al., 2019; Ovadnevaite et al., 2017; Schmedding et al., 2023; Vepsäläinen et al., 2022). Accounting for phase separation in predicting hygroscopic growth of cloud condensation nuclei (CCN) resulted in an increase in the super-saturation % required for CCN activation (Davies et al., 2019); however, the presence of organics and liquid-liquid phase separation has been seen to lower the surface tension of liquid particles and reduces underpredictions in CCN (Ovadnevaite et al., 2017). Further theoretical work has found that liquid-liquid phase separation with a thin organic film can result in substantial CCN activation (Schmedding et al., 2023; Vepsäläinen et al., 2022) for smaller particles (Schmedding et al., 2023). All of the above point to the impacts of liquid-liquid phase separation on low-lying cloud formation and opacity, which are also recent avenues for model improvement in predicting the radiative budget (Szopa et al., 2023). In addition, phase separation has recently been shown to also impact the radiative properties of some aerosols (Fard et al., 2018; Zhang et al., 2022). Fard et al., (2018) found that liquid-liquid phase separation in brown carbon aerosols increased their scattering cross-sections and decreased their absorbing cross-sections (Fard et al., 2018). Zhang et al., (2022) found that with increasing organic coatings in a phase separated aerosol, that black carbon absorption decreased (Zhang et al., 2022). Accounting for phase separation can impact the potency of aerosols as short-lived climate forcers (Fard et al., 2018; Zhang et al., 2022) and have the potential to influence meteorological predictions, and consequently pollutant concentrations in meteorological-chemical coupled transport models (Forkel et al., 2015; Gao et al., 2024; Hogrefe et al., 2015; Wang et al., 2021; Wong et al., 2012).

Accounting for phase state and phase separation also has the potential to extend the atmospheric life-times (i.e., semi-solid or solid phase state) and thus transport of harmful air pollutants (HAPs) (Mu et al., 2018; Shrivastava et al., 2017). Shrivastava et al. (2017) found that accounting for aged organic coatings resolved model-measurements gaps of Benzo[a]pyrene (BaP), a HAP with lung carcinogenicity (Boström et al., 2002; Bukowska et al., 2022), suggesting shielding from the organic coating limits photo-oxidant degradation. Mu et al. (2018) found that the lifetime of BaP (against ozone) in phase-separated aerosols decreases with increased RH (Mu et al., 2018). Both of these studies highlight the importance of long-range transport of HAPs that can harm human health particularly in the mid-to-upper latitudes (Mu et al., 2018; Shrivastava et al., 2017) and highlight the importance of accurately predicting phase separation and phase state in air quality models.

https://doi.org/10.5194/egusphere-2025-2253
Preprint. Discussion started: 5 August 2025
© Author(s) 2025. CC BY 4.0 License.

## 5 Conclusion

Although inorganic-organic phase separation and phase state of aerosols, is known to happen (Riva et al., 2019; Zhang et al., 2019a), these physical properties are not traditionally included in chemical transport models, yet can impact heterogeneous aerosol formation. In this work, we demonstrate that the phase state of phase separated aerosols can decrease the heterogeneous reactive uptake of IEPOX and subsequent formation of IEPOX-SOA. This decrease is largely attributed to a more solid phase state of the outer organic shell (Fig. 3a-c, Fig. 6). While this reduction overall furthers a negative bias in simulating total IEPOX-SOA, and explicitly tracked methyltetrol sulfates (AIEOS), it reduces a positive bias in simulating explicitly tracked 2-methyltetrols (AIETET). We find that with increased ALW associated with the outer organic shell, its phase state is more liquid-like and does not pose as much of a diffusional resistance to heterogeneous reactive uptake. The simulated phase states (also modulated by $T_g$ parameterization used), can be used as bounds for SAPRC07tic_ae7i organic aerosol species in future studies. Within each phase state parameterization, future modeling studies should also aim to update model organic aerosol properties ($C^0, M,$ and $O:C$) upon which phase state parameterizations rely. Ultimately phase separation and phase state of aerosols have implications beyond impacting heterogeneous chemistry and more field measurements of aerosol phase state are warranted to further validate the organic aerosol phase states simulated in this study.

## Code/Data Availability

The version of CMAQ used in this paper, CMAQv5.3.2, is archived at https://doi.org/10.5281/zenodo.4081737 (USEPA Office of Research and Development, 2020) and is used for the base model runs. Sensitivity model cases were developed on top of the base model setup with additional coding contributions from Quazi Z. Rasool and Sara Farrell and can be accessed at https://github.com/slfarrell/ACP_IEPOX_Coatings_paper along with both output data and analysis code used to generate figures.

## Author Contribution

SF, QZR, HOTP, WV, RS, YZ, YL, and YC were responsible for conceptualization. WV, JDS, MS, and JLJ were responsible for funding acquisition. QZR, SF, HOTP, and RS were responsible for CMAQ model software development. SF, QZR, and CW were responsible for data analysis and model validation. HZ, SB, JDS, WH, and JLJ were responsible for measurements used for CMAQ model evaluation. SF and WV were responsible for writing the original draft. All co-authors contributed to writing – review and editing.

## Competing Interests

MS is a member of the editorial board of the journal ACP.

## Disclaimer

https://doi.org/10.5194/egusphere-2025-2253
Preprint. Discussion started: 5 August 2025
© Author(s) 2025. CC BY 4.0 License.

The views expressed in this article are those of the authors and do not necessarily represent the views or policies of the US Environmental Protection Agency, the University of North Carolina at Chapel Hill, Texas A&M University, the University of California – Irvine, Chinese Academy of Sciences, George Mason University, University of California – Riverside, McGill University, the University of York, nor the University of Colorado – Boulder.

**Acknowledgments**

MS thanks funding from the U.S. National Science Foundation (NSF) under a grant from the Division of Atmospheric and Geospace Sciences (AGS-2246502). WV thanks funding from U.S. NSF grant AGS-2037697. JDS thanks funding from U.S. NSF grant AGS-2039788. YL thanks the funding from National Natural Science Foundation of China (grant nos. 42075110 and 42475124). YZ thanks the funding from the U.S. NSF Postdoctoral Fellowship (AGS-152473) and grant AGS-2131369. SLF thanks the National Institute for Occupational Health for partial funding of this work, and Kathleen Fahey and Ivan Piletic for their thorough reviews and suggestions for this paper. HZ thanks the funding from the U.S. NSF grant AGS-2037698.

**References**

Abbott, T. H., & Cronin, T. W. Aerosol invigoration of atmospheric convection through increases in humidity. *Science, 371*(6524), 83-85. doi:10.1126/science.abc5181 (2021).

Anderson, E. V., G.D.; Weininger, D. (1987). *SMILES: A line notation and computerized interpreter for chemical structures*. Retrieved from

Appel, K. W., Bash, J. O., Fahey, K. M., Foley, K. M., Gilliam, R. C., Hogrefe, C., Hutzell, W. T., Kang, D., Mathur, R., Murphy, B. N., Napelenok, S. L., Nolte, C. G., Pleim, J. E., Pouliot, G. A., Pye, H. O. T., Ran, L., Roselle, S. J., Sarwar, G., Schwede, D. B., Sidi, F. I., Spero, T. L., & Wong, D. C. The Community Multiscale Air Quality (CMAQ) Model Versions 5.3 and 5.3.1: System Updates and Evaluation. *Geosci. Model Dev. Discuss., 2020*, 1-41. doi:10.5194/gmd-2020-345 (2020).

Appel, K. W., Napelenok, S. L., Foley, K. M., Pye, H. O. T., Hogrefe, C., Luecken, D. J., Bash, J. O., Roselle, S. J., Pleim, J. E., Foroutan, H., Hutzell, W. T., Pouliot, G. A., Sarwar, G., Fahey, K. M., Gantt, B., Gilliam, R. C., Heath, N. K., Kang, D., Mathur, R., Schwede, D. B., Spero, T. L., Wong, D. C., & Young, J. O. Description and evaluation of the Community Multiscale Air Quality (CMAQ) modeling system version 5.1. *Geosci. Model Dev., 10*(4), 1703-1732. doi:10.5194/gmd-10-1703-2017 (2017).

Armstrong, N. C., Chen, Y., Cui, T., Zhang, Y., Christensen, C., Zhang, Z., Turpin, B. J., Chan, M. N., Gold, A., Ault, A. P., & Surratt, J. D. Isoprene Epoxydiol-Derived Sulfated and Nonsulfated Oligomers Suppress Particulate Mass Loss during Oxidative Aging of Secondary Organic Aerosol. *Environmental Science & Technology, 56*(23), 16611-16620. doi:10.1021/acs.est.2c03200 (2022).

Berkemeier, T., Shiraiwa, M., Pöschl, U., & Koop, T. Competition between water uptake and ice nucleation by glassy organic aerosol particles. *Atmos. Chem. Phys., 14*(22), 12513-12531. doi:10.5194/acp-14-12513-2014 (2014).

Bertram, A. K., Martin, S. T., Hanna, S. J., Smith, M. L., Bodsworth, A., Chen, Q., Kuwata, M., Liu, A., You, Y., & Zorn, S. R. Predicting the relative humidities of liquid-liquid phase separation, efflorescence, and deliquescence of mixed particles of ammonium sulfate, organic material, and water using the organic-to-sulfate mass ratio of the particle and the oxygen-to-carbon elemental ratio of the organic component. *Atmos. Chem. Phys., 11*(21), 10995-11006. doi:10.5194/acp-11-10995-2011 (2011).

Boström, C. E., Gerde, P., Hanberg, A., Jernström, B., Johansson, C., Kyrklund, T., Rannug, A., Törnqvist, M., Victorin, K., & Westerholm, R. Cancer risk assessment, indicators, and guidelines for polycyclic aromatic hydrocarbons in the ambient air. *Environ Health Perspect, 110 Suppl 3*(Suppl 3), 451-488. doi:10.1289/ehp.110-1241197 (2002).

https://doi.org/10.5194/egusphere-2025-2253
Preprint. Discussion started: 5 August 2025
© Author(s) 2025. CC BY 4.0 License.

Brüggemann, M., Xu, R., Tilgner, A., Kwong, K. C., Mutzel, A., Poon, H. Y., Otto, T., Schaefer, T., Poulain, L., Chan, M. N., & Herrmann, H. Organosulfates in Ambient Aerosol: State of Knowledge and Future Research Directions on Formation, Abundance, Fate, and Importance. *Environmental Science & Technology, 54*(7), 3767-3782. doi:10.1021/acs.est.9b06751 (2020).

Budisulistiorini, S. H., Li, X., Bairai, S. T., Renfro, J., Liu, Y., Liu, Y. J., McKinney, K. A., Martin, S. T., McNeill, V. F., Pye, H. O. T., Nenes, A., Neff, M. E., Stone, E. A., Mueller, S., Knote, C., Shaw, S. L., Zhang, Z., Gold, A., & Surratt, J. D. Examining the effects of anthropogenic emissions on isoprene-derived secondary organic aerosol formation during the 2013 Southern Oxidant and Aerosol Study (SOAS) at the Look Rock, Tennessee ground site. *Atmospheric Chemistry and Physics, 15*(15), 8871-8888. doi:http://dx.doi.org/10.5194/acp-15-8871-2015 (2015a).

Budisulistiorini, S. H., Li, X., Bairai, S. T., Renfro, J., Liu, Y., Liu, Y. J., McKinney, K. A., Martin, S. T., McNeill, V. F., Pye, H. O. T., Nenes, A., Neff, M. E., Stone, E. A., Mueller, S., Knote, C., Shaw, S. L., Zhang, Z., Gold, A., & Surratt, J. D. Examining the effects of anthropogenic emissions on isoprene-derived secondary organic aerosol formation during the 2013 Southern Oxidant and Aerosol Study (SOAS) at the Look Rock, Tennessee ground site. *Atmos. Chem. Phys., 15*(15), 8871-8888. doi:10.5194/acp-15-8871-2015 (2015b).

Budisulistiorini, S. H., Nenes, A., Carlton, A. G., Surratt, J. D., McNeill, V. F., & Pye, H. O. T. Simulating Aqueous-Phase Isoprene-Epoxydiol (IEPOX) Secondary Organic Aerosol Production During the 2013 Southern Oxidant and Aerosol Study (SOAS). *Environmental Science & Technology, 51*(9), 5026-5034. doi:10.1021/acs.est.6b05750 (2017).

Bukowska, B., Mokra, K., & Michałowicz, J. Benzo[a]pyrene—Environmental Occurrence, Human Exposure, and Mechanisms of Toxicity. *International Journal of Molecular Sciences, 23*(11), 6348. Retrieved from https://www.mdpi.com/1422-0067/23/11/6348(2022).

Chen, B., Mirrielees, J. A., Chen, Y., Onasch, T. B., Zhang, Z., Gold, A., Surratt, J. D., Zhang, Y., & Brooks, S. D. Glass Transition Temperatures of Organic Mixtures from Isoprene Epoxydiol-Derived Secondary Organic Aerosol. *The Journal of Physical Chemistry A, 127*(18), 4125-4136. doi:10.1021/acs.jpca.2c08936 (2023).

Chen, Y., Dombek, T., Hand, J., Zhang, Z., Gold, A., Ault, A. P., Levine, K. E., & Surratt, J. D. Seasonal Contribution of Isoprene-Derived Organosulfates to Total Water-Soluble Fine Particulate Organic Sulfur in the United States. *ACS Earth and Space Chemistry, 5*(9), 2419-2432. doi:10.1021/acsearthspacechem.1c00102 (2021).

Chen, Y., Ng, A. E., Green, J., Zhang, Y., Riva, M., Riedel, T. P., Pye, H. O. T., Lei, Z., Olson, N. E., Cooke, M. E., Zhang, Z., Vizuete, W., Gold, A., Turpin, B. J., Ault, A. P., & Surratt, J. D. Applying a Phase-Separation Parameterization in Modeling Secondary Organic Aerosol Formation from Acid-Driven Reactive Uptake of Isoprene Epoxydiols under Humid Conditions. *ACS ES&T Air, 1*(6), 511-524. doi:10.1021/acsestair.4c00002 (2024).

Compernolle, S., Ceulemans, K., & Müller, J. F. EVAPORATION: a new vapour pressure estimation methodfor organic molecules including non-additivity and intramolecular interactions. *Atmospheric Chemistry and Physics, 11*(18), 9431. Retrieved from http://libproxy.lib.unc.edu/login?url=https://www.proquest.com/scholarly-journals/evaporation-new-vapour-pressure-estimation/docview/890078804/se-2?accountid=14244
http://VB3LK7EB4T.search.serialssolutions.com/?genre=article&atitle=EVAPORATION%3A+a+new+vapour+pressure+estimation+methodfor+organic+molecules+including+non-additivity+and+intramolecular+interactions&author=Compernolle%2C+S.%3BCeulemans%2C+K.%3BM%C3%BCller%2C+J.-F.&volume=11&issue=18&spage=9431&date=2011&rft.btitle=&rft.jtitle=Atmospheric+Chemistry+and+Physics&issn=1680-7316&isbn=&sid=ProQ%3Ahightechjournals_(2011).

Cooke, M. E., Armstrong, N. C., Fankhauser, A. M., Chen, Y., Lei, Z., Zhang, Y., Ledsky, I. R., Turpin, B. J., Zhang, Z., Gold, A., McNeill, V. F., Surratt, J. D., & Ault, A. P. Decreases in Epoxide-Driven Secondary Organic Aerosol Production under Highly Acidic Conditions: The Importance of Acid–Base Equilibria. *Environmental Science & Technology, 58*(24), 10675-10684. doi:10.1021/acs.est.3c10851 (2024).

Cziczo, D. J., Froyd, K. D., Hoose, C., Jensen, E. J., Diao, M., Zondlo, M. A., Smith, J. B., Twohy, C. H., & Murphy, D. M. Clarifying the Dominant Sources and Mechanisms of Cirrus Cloud Formation. *Science, 340*(6138), 1320-1324. doi:10.1126/science.1234145 (2013).

D'Ambro, E. L., Schobesberger, S., Gaston, C. J., Lopez-Hilfiker, F. D., Lee, B. H., Liu, J., Zelenyuk, A., Bell, D., Cappa, C. D., Helgestad, T., Li, Z., Guenther, A., Wang, J., Wise, M., Caylor, R., Surratt, J. D., Riedel, T., Hyttinen, N., Salo, V. T., Hasan, G., Kurtén, T., Shilling, J. E., & Thornton, J. A. Chamber-based insights into the factors controlling

© Author(s) 2025. CC BY 4.0 License.

epoxydiol (IEPOX) secondary organic aerosol (SOA) yield, composition, and volatility. *Atmos. Chem. Phys., 19*(17), 11253-11265. doi:10.5194/acp-19-11253-2019 (2019).

Davies, J. F., Zuend, A., & Wilson, K. R. Technical note: The role of evolving surface tension in the formation of cloud droplets. *Atmos. Chem. Phys., 19*(5), 2933-2946. doi:10.5194/acp-19-2933-2019 (2019).

DeRieux, W. S. W., Li, Y., Lin, P., Laskin, J., Laskin, A., Bertram, A. K., Nizkorodov, S. A., & Shiraiwa, M. Predicting the glass transition temperature and viscosity of secondary organic material using molecular composition. *Atmos. Chem. Phys., 18*(9), 6331-6351. doi:10.5194/acp-18-6331-2018 (2018).

Dette, H. P., Qi, M., Schröder, D. C., Godt, A., & Koop, T. Glass-Forming Properties of 3-Methylbutane-1,2,3-tricarboxylic Acid and Its Mixtures with Water and Pinonic Acid. *The Journal of Physical Chemistry A, 118*(34), 7024-7033. doi:10.1021/jp505910w (2014).

Donahue, N. M., Robinson, A. L., Stanier, C. O., & Pandis, S. N. Coupled Partitioning, Dilution, and Chemical Aging of Semivolatile Organics. *Environmental Science & Technology, 40*(8), 2635-2643. doi:10.1021/es052297c (2006).

Eddingsaas, N. C., VanderVelde, D. G., & Wennberg, P. O. Kinetics and products of the acid-catalyzed ring-opening of atmospherically relevant butyl epoxy alcohols. *J Phys Chem A, 114*(31), 8106-8113. doi:10.1021/jp103907c (2010).

Estimation Programs Interface for Microsoft Windows. (2012). EPA, U. S. (Version 4.11) [Mobile application software]

Fard, M. M., Krieger, U. K., & Peter, T. Shortwave radiative impact of liquid–liquid phase separation in brown carbon aerosols. *Atmos. Chem. Phys., 18*(18), 13511-13530. doi:10.5194/acp-18-13511-2018 (2018).

Farrell, S. L., Pye, H. O. T., Gilliam, R., Pouliot, G., Huff, D., Sarwar, G., Vizuete, W., Briggs, N., & Fahey, K. Predicted impacts of heterogeneous chemical pathways on particulate sulfur over Fairbanks, Alaska, the N. Hemisphere, and the Contiguous United States. *EGUsphere, 2024*, 1-43. doi:10.5194/egusphere-2024-1550 (2024).

Forkel, R., Balzarini, A., Baró, R., Bianconi, R., Curci, G., Jiménez-Guerrero, P., Hirtl, M., Honzak, L., Lorenz, C., Im, U., Pérez, J. L., Pirovano, G., San José, R., Tuccella, P., Werhahn, J., & Žabkar, R. Analysis of the WRF-Chem contributions to AQMEII phase2 with respect to aerosol radiative feedbacks on meteorology and pollutant distributions. *Atmospheric Environment, 115*, 630-645. doi:https://doi.org/10.1016/j.atmosenv.2014.10.056 (2015).

Fulcher, G. S. ANALYSIS OF RECENT MEASUREMENTS OF THE VISCOSITY OF GLASSES. *Journal of the American Ceramic Society, 8*(6), 339-355. doi:https://doi.org/10.1111/j.1151-2916.1925.tb16731.x (1925).

Gao, C., Zhang, X., Xiu, A., Tong, Q., Zhao, H., Zhang, S., Yang, G., Zhang, M., & Xie, S. Intercomparison of multiple two-way coupled meteorology and air quality models (WRF v4.1.1–CMAQ v5.3.1, WRF–Chem v4.1.1, and WRF v3.7.1–CHIMERE v2020r1) in eastern China. *Geosci. Model Dev., 17*(6), 2471-2492. doi:10.5194/gmd-17-2471-2024 (2024).

Gaston, C. J., Riedel, T. P., Zhang, Z., Gold, A., Surratt, J. D., & Thornton, J. A. Reactive Uptake of an Isoprene-Derived Epoxydiol to Submicron Aerosol Particles. *Environmental Science & Technology, 48*(19), 11178-11186. doi:10.1021/es5034266 (2014).

Guenther, A., Karl, T., Harley, P., Wiedinmyer, C., Palmer, P. I., & Geron, C. Estimates of global terrestrial isoprene emissions using MEGAN (Model of Emissions of Gases and Aerosols from Nature). *Atmos. Chem. Phys., 6*(11), 3181-3210. doi:10.5194/acp-6-3181-2006 (2006).

Guenther, A. B., Jiang, X., Heald, C. L., Sakulyanontvittaya, T., Duhl, T., Emmons, L. K., & Wang, X. The Model of Emissions of Gases and Aerosols from Nature version 2.1 (MEGAN2.1): an extended and updated framework for modeling biogenic emissions. *Geosci. Model Dev., 5*(6), 1471-1492. doi:10.5194/gmd-5-1471-2012 (2012).

Hallquist, M., Wenger, J. C., Baltensperger, U., Rudich, Y., Simpson, D., Claeys, M., Dommen, J., Donahue, N. M., George, C., Goldstein, A. H., Hamilton, J. F., Herrmann, H., Hoffmann, T., Iinuma, Y., Jang, M., Jenkin, M. E., Jimenez, J. L., Kiendler-Scharr, A., Maenhaut, W., McFiggans, G., Mentel, T. F., Monod, A., Prévôt, A. S. H., Seinfeld, J. H., Surratt, J. D., Szmigielski, R., & Wildt, J. The formation, properties and impact of secondary organic aerosol: current and emerging issues. *Atmos. Chem. Phys., 9*(14), 5155-5236. doi:10.5194/acp-9-5155-2009 (2009).

Heath, N. K., Pleim, J. E., Gilliam, R. C., & Kang, D. A simple lightning assimilation technique for improving retrospective WRF simulations. *Journal of Advances in Modeling Earth Systems, 8*(4), 1806-1824. doi:https://doi.org/10.1002/2016MS000735 (2016).

Hogrefe, C., Pouliot, G., Wong, D., Torian, A., Roselle, S., Pleim, J., & Mathur, R. Annual application and evaluation of the online coupled WRF–CMAQ system over North America under AQMEII phase 2. *Atmospheric Environment, 115*, 683-694. doi:https://doi.org/10.1016/j.atmosenv.2014.12.034 (2015).

https://doi.org/10.5194/egusphere-2025-2253
Preprint. Discussion started: 5 August 2025
© Author(s) 2025. CC BY 4.0 License.

Hu, W., Palm, B. B., Day, D. A., Campuzano-Jost, P., Krechmer, J. E., Peng, Z., de Sá, S. S., Martin, S. T., Alexander, M. L., Baumann, K., Hacker, L., Kiendler-Scharr, A., Koss, A. R., de Gouw, J. A., Goldstein, A. H., Seco, R., Sjostedt, S. J., Park, J. H., Guenther, A. B., Kim, S., Canonaco, F., Prévôt, A. S. H., Brune, W. H., & Jimenez, J. L. Volatility and lifetime against OH heterogeneous reaction of ambient isoprene-epoxydiols-derived secondary organic aerosol (IEPOX-SOA). *Atmos. Chem. Phys., 16*(18), 11563-11580. doi:10.5194/acp-16-11563-2016 (2016).

Hyttinen, N., Elm, J., Malila, J., Calderón, S. M., & Prisle, N. L. Thermodynamic properties of isoprene- and monoterpene-derived organosulfates estimated with COSMOtherm. *Atmos. Chem. Phys., 20*(9), 5679-5696. doi:10.5194/acp-20-5679-2020 (2020).

Jang, M., Czoschke, N. M., Lee, S., & Kamens, R. M. Heterogeneous Atmospheric Aerosol Production by Acid-Catalyzed Particle-Phase Reactions. *Science, 298*(5594), 814-817. doi:10.1126/science.1075798 (2002).

Jimenez, J. L., Canagaratna, M. R., Donahue, N. M., Prevot, A. S. H., Zhang, Q., Kroll, J. H., DeCarlo, P. F., Allan, J. D., Coe, H., Ng, N. L., Aiken, A. C., Docherty, K. S., Ulbrich, I. M., Grieshop, A. P., Robinson, A. L., Duplissy, J., Smith, J. D., Wilson, K. R., Lanz, V. A., Hueglin, C., Sun, Y. L., Tian, J., Laaksonen, A., Raatikainen, T., Rautiainen, J., Vaattovaara, P., Ehn, M., Kulmala, M., Tomlinson, J. M., Collins, D. R., Cubison, M. J., Dunlea, J., Huffman, J. A., Onasch, T. B., Alfarra, M. R., Williams, P. I., Bower, K., Kondo, Y., Schneider, J., Drewnick, F., Borrmann, S., Weimer, S., Demerjian, K., Salcedo, D., Cottrell, L., Griffin, R., Takami, A., Miyoshi, T., Hatakeyama, S., Shimono, A., Sun, J. Y., Zhang, Y. M., Dzepina, K., Kimmel, J. R., Sueper, D., Jayne, J. T., Herndon, S. C., Trimborn, A. M., Williams, L. R., Wood, E. C., Middlebrook, A. M., Kolb, C. E., Baltensperger, U., & Worsnop, D. R. Evolution of Organic Aerosols in the Atmosphere. *Science, 326*(5959), 1525-1529. doi:10.1126/science.1180353 (2009).

Jo, D. S., Hodzic, A., Emmons, L. K., Tilmes, S., Schwantes, R. H., Mills, M. J., Campuzano-Jost, P., Hu, W., Zaveri, R. A., Easter, R. C., Singh, B., Lu, Z., Schulz, C., Schneider, J., Shilling, J. E., Wisthaler, A., & Jimenez, J. L. Future changes in isoprene-epoxydiol-derived secondary organic aerosol (IEPOX SOA) under the Shared Socioeconomic Pathways: the importance of physicochemical dependency. *Atmos. Chem. Phys., 21*(5), 3395-3425. doi:10.5194/acp-21-3395-2021 (2021).

Koop, T., Bookhold, J., Shiraiwa, M., & Pöschl, U. Glass transition and phase state of organic compounds: dependency on molecular properties and implications for secondary organic aerosols in the atmosphere. *Physical Chemistry Chemical Physics, 13*(43), 19238-19255. doi:10.1039/C1CP22617G (2011).

Kulmala, M., Kontkanen, J., Junninen, H., Lehtipalo, K., Manninen, H. E., Nieminen, T., Petäjä, T., Sipilä, M., Schobesberger, S., Rantala, P., Franchin, A., Jokinen, T., Järvinen, E., Äijälä, M., Kangasluoma, J., Hakala, J., Aalto, P. P., Paasonen, P., Mikkilä, J., Vanhanen, J., Aalto, J., Hakola, H., Makkonen, U., Ruuskanen, T., Mauldin, R. L., Duplissy, J., Vehkamäki, H., Bäck, J., Kortelainen, A., Riipinen, I., Kurtén, T., Johnston, M. V., Smith, J. N., Ehn, M., Mentel, T. F., Lehtinen, K. E. J., Laaksonen, A., Kerminen, V.-M., & Worsnop, D. R. Direct Observations of Atmospheric Aerosol Nucleation. *Science, 339*(6122), 943-946. doi:10.1126/science.1227385 (2013).

Kurtén, T., Tiusanen, K., Roldin, P., Rissanen, M., Luy, J.-N., Boy, M., Ehn, M., & Donahue, N. α-Pinene Autoxidation Products May Not Have Extremely Low Saturation Vapor Pressures Despite High O:C Ratios. *The Journal of Physical Chemistry A, 120*(16), 2569-2582. doi:10.1021/acs.jpca.6b02196 (2016).

Li, Y., Carlton, A. G., & Shiraiwa, M. Diurnal and Seasonal Variations in the Phase State of Secondary Organic Aerosol Material over the Contiguous US Simulated in CMAQ. *ACS Earth and Space Chemistry, 5*(8), 1971-1982. doi:10.1021/acsearthspacechem.1c00094 (2021).

Li, Y., Day, D. A., Stark, H., Jimenez, J. L., & Shiraiwa, M. Predictions of the glass transition temperature and viscosity of organic aerosols from volatility distributions. *Atmos. Chem. Phys., 20*(13), 8103-8122. doi:10.5194/acp-20-8103-2020 (2020).

Lilek, J., & Zuend, A. A predictive viscosity model for aqueous electrolytes and mixed organic–inorganic aerosol phases. *Atmos. Chem. Phys., 22*(5), 3203-3233. doi:10.5194/acp-22-3203-2022 (2022).

Lin, Y.-H., Zhang, H., Pye, H. O. T., Zhang, Z., Marth, W. J., Park, S., Arashiro, M., Cui, T., Budisulistiorini, S. H., Sexton, K. G., Vizuete, W., Xie, Y., Luecken, D. J., Piletic, I. R., Edney, E. O., Bartolotti, L. J., Gold, A., & Surratt, J. D. Epoxide as a precursor to secondary organic aerosol formation from isoprene photooxidation in the presence of nitrogen oxides. *Proceedings of the National Academy of Sciences, 110*(17), 6718-6723. doi:10.1073/pnas.1221150110 (2013).

https://doi.org/10.5194/egusphere-2025-2253
Preprint. Discussion started: 5 August 2025
© Author(s) 2025. CC BY 4.0 License.

Luu, R., Schervish, M., June, N. A., O'Donnell, S. E., Jathar, S. H., Pierce, J. R., & Shiraiwa, M. Global Simulations of Phase State and Equilibration Time Scales of Secondary Organic Aerosols with GEOS-Chem. *ACS Earth and Space Chemistry, 9*(2), 288-302. doi:10.1021/acsearthspacechem.4c00281 (2025).

Maclean, A. M., Li, Y., Crescenzo, G. V., Smith, N. R., Karydis, V. A., Tsimpidi, A. P., Butenhoff, C. L., Faiola, C. L., Lelieveld, J., Nizkorodov, S. A., Shiraiwa, M., & Bertram, A. K. Global Distribution of the Phase State and Mixing Times within Secondary Organic Aerosol Particles in the Troposphere Based on Room-Temperature Viscosity Measurements. *ACS Earth and Space Chemistry, 5*(12), 3458-3473. doi:10.1021/acsearthspacechem.1c00296 (2021).

Mansouri, K., Grulke, C. M., Judson, R. S., & Williams, A. J. OPERA models for predicting physicochemical properties and environmental fate endpoints. *Journal of Cheminformatics, 10*(1), 10. doi:10.1186/s13321-018-0263-1 (2018).

McNeill, V. F. Aqueous Organic Chemistry in the Atmosphere: Sources and Chemical Processing of Organic Aerosols. *Environmental Science & Technology, 49*(3), 1237-1244. doi:10.1021/es5043707 (2015).

Miller, C. C. The Stokes-Einstein Law for Diffusion in Solution. *Proceedings of the Royal Society of London. Series A, Containing Papers of a Mathematical and Physical Character, 106*(740), 724-749. Retrieved from http://www.jstor.org/stable/94335(1924).

Mu, Q., Shiraiwa, M., Octaviani, M., Ma, N., Ding, A., Su, H., Lammel, G., Pöschl, U., & Cheng, Y. Temperature effect on phase state and reactivity controls atmospheric multiphase chemistry and transport of PAHs. *Science Advances, 4*(3), eaap7314. doi:10.1126/sciadv.aap7314 (2018).

Murray, B. J., Wilson, T. W., Dobbie, S., Cui, Z., Al-Jumur, S. M. R. K., Möhler, O., Schnaiter, M., Wagner, R., Benz, S., Niemand, M., Saathoff, H., Ebert, V., Wagner, S., & Kärcher, B. Heterogeneous nucleation of ice particles on glassy aerosols under cirrus conditions. *Nature Geoscience, 3*(4), 233-237. doi:10.1038/ngeo817 (2010).

Nozière, B., Kalberer, M., Claeys, M., Allan, J., D'Anna, B., Decesari, S., Finessi, E., Glasius, M., Grgić, I., Hamilton, J. F., Hoffmann, T., Iinuma, Y., Jaoui, M., Kahnt, A., Kampf, C. J., Kourtchev, I., Maenhaut, W., Marsden, N., Saarikoski, S., Schnelle-Kreis, J., Surratt, J. D., Szidat, S., Szmigielski, R., & Wisthaler, A. The Molecular Identification of Organic Compounds in the Atmosphere: State of the Art and Challenges. *Chemical Reviews, 115*(10), 3919-3983. doi:10.1021/cr5003485 (2015).

Octaviani, M., Shrivastava, M., Zaveri, R. A., Zelenyuk, A., Zhang, Y., Rasool, Q. Z., Bell, D. M., Riva, M., Glasius, M., & Surratt, J. D. Modeling the Size Distribution and Chemical Composition of Secondary Organic Aerosols during the Reactive Uptake of Isoprene-Derived Epoxydiols under Low-Humidity Condition. *ACS Earth and Space Chemistry, 5*(11), 3247-3257. doi:10.1021/acsearthspacechem.1c00303 (2021).

Odum, J. R., Hoffmann, T., Bowman, F., Collins, D., Flagan, R. C., & Seinfeld, J. H. Gas/Particle Partitioning and Secondary Organic Aerosol Yields. *Environmental Science & Technology, 30*(8), 2580-2585. doi:10.1021/es950943+ (1996).

Olson, N. E., Lei, Z., Craig, R. L., Zhang, Y., Chen, Y., Lambe, A. T., Zhang, Z., Gold, A., Surratt, J. D., & Ault, A. P. Reactive Uptake of Isoprene Epoxydiols Increases the Viscosity of the Core of Phase-Separated Aerosol Particles. *ACS Earth and Space Chemistry, 3*(8), 1402-1414. doi:10.1021/acsearthspacechem.9b00138 (2019).

Ovadnevaite, J., Zuend, A., Laaksonen, A., Sanchez, K. J., Roberts, G., Ceburnis, D., Decesari, S., Rinaldi, M., Hodas, N., Facchini, M. C., Seinfeld, J. H., & C, O. D. Surface tension prevails over solute effect in organic-influenced cloud droplet activation. *Nature, 546*(7660), 637-641. doi:10.1038/nature22806 (2017).

Paciga, A. L., Riipinen, I., & Pandis, S. N. Effect of Ammonia on the Volatility of Organic Diacids. *Environmental Science & Technology, 48*(23), 13769-13775. doi:10.1021/es5037805 (2014).

Pankow, J. F. An absorption model of the gas/aerosol partitioning involved in the formation of secondary organic aerosol. *Atmospheric Environment, 28*(2), 189-193. doi:https://doi.org/10.1016/1352-2310(94)90094-9 (1994).

Paulot, F., Crounse, J. D., Kjaergaard, H. G., Kürten, A., St Clair, J. M., Seinfeld, J. H., & Wennberg, P. O. Unexpected epoxide formation in the gas-phase photooxidation of isoprene. *Science, 325*(5941), 730-733. doi:10.1126/science.1172910 (2009).

Petters, S. S., Cui, T., Zhang, Z., Gold, A., McNeill, V. F., Surratt, J. D., & Turpin, B. J. Organosulfates from Dark Aqueous Reactions of Isoprene-Derived Epoxydiols Under Cloud and Fog Conditions: Kinetics, Mechanism, and Effect of Reaction Environment on Regioselectivity of Sulfate Addition. *ACS Earth and Space Chemistry, 5*(3), 474-486. doi:10.1021/acsearthspacechem.0c00293 (2021).

Piletic, I. R., Edney, E. O., & Bartolotti, L. J. A computational study of acid catalyzed aerosol reactions of atmospherically relevant epoxides. *Physical Chemistry Chemical Physics, 15*(41), 18065-18076. doi:10.1039/C3CP52851K (2013).

https://doi.org/10.5194/egusphere-2025-2253
Preprint. Discussion started: 5 August 2025
© Author(s) 2025. CC BY 4.0 License.

Pye, H. O. T., Luecken, D. J., Xu, L., Boyd, C. M., Ng, N. L., Baker, K. R., Ayres, B. R., Bash, J. O., Baumann, K., Carter, W. P. L., Edgerton, E., Fry, J. L., Hutzell, W. T., Schwede, D. B., & Shepson, P. B. Modeling the Current and Future Roles of Particulate Organic Nitrates in the Southeastern United States. *Environmental Science & Technology, 49*(24), 14195-14203. doi:10.1021/acs.est.5b03738 (2015).

Pye, H. O. T., Murphy, B. N., Xu, L., Ng, N. L., Carlton, A. G., Guo, H., Weber, R., Vasilakos, P., Appel, K. W., Budisulistiorini, S. H., Surratt, J. D., Nenes, A., Hu, W., Jimenez, J. L., Isaacman-VanWertz, G., Misztal, P. K., & Goldstein, A. H. On the implications of aerosol liquid water and phase separation for organic aerosol mass. *Atmos. Chem. Phys., 17*(1), 343-369. doi:10.5194/acp-17-343-2017 (2017).

Pye, H. O. T., Pinder, R. W., Piletic, I. R., Xie, Y., Capps, S. L., Lin, Y.-H., Surratt, J. D., Zhang, Z., Gold, A., Luecken, D. J., Hutzell, W. T., Jaoui, M., Offenberg, J. H., Kleindienst, T. E., Lewandowski, M., & Edney, E. O. Epoxide Pathways Improve Model Predictions of Isoprene Markers and Reveal Key Role of Acidity in Aerosol Formation. *Environmental Science & Technology, 47*(19), 11056-11064. doi:10.1021/es402106h (2013).

Pye, H. O. T., Place, B. K., Murphy, B. N., Seltzer, K. M., D'Ambro, E. L., Allen, C., Piletic, I. R., Farrell, S., Schwantes, R. H., Coggon, M. M., Saunders, E., Xu, L., Sarwar, G., Hutzell, W. T., Foley, K. M., Pouliot, G., Bash, J., & Stockwell, W. R. Linking gas, particulate, and toxic endpoints to air emissions in the Community Regional Atmospheric Chemistry Multiphase Mechanism (CRACMM). *Atmos. Chem. Phys., 23*(9), 5043-5099. doi:10.5194/acp-23-5043-2023 (2023).

Pye, H. O. T., Ward-Caviness, C. K., Murphy, B. N., Appel, K. W., & Seltzer, K. M. Secondary organic aerosol association with cardiorespiratory disease mortality in the United States. *Nature Communications, 12*(1), 7215. doi:10.1038/s41467-021-27484-1 (2021).

Rasool, Q. Z., Shrivastava, M., Octaviani, M., Zhao, B., Gaudet, B., & Liu, Y. Modeling Volatility-Based Aerosol Phase State Predictions in the Amazon Rainforest. *ACS Earth and Space Chemistry, 5*(10), 2910-2924. doi:10.1021/acsearthspacechem.1c00255 (2021).

Riedel, T. P., Lin, Y.-H., Budisulistiorini, S. H., Gaston, C. J., Thornton, J. A., Zhang, Z., Vizuete, W., Gold, A., & Surratt, J. D. Heterogeneous Reactions of Isoprene-Derived Epoxides: Reaction Probabilities and Molar Secondary Organic Aerosol Yield Estimates. *Environmental Science & Technology Letters, 2*(2), 38-42. doi:10.1021/ez500406f (2015).

Riedel, T. P., Lin, Y. H., Zhang, Z., Chu, K., Thornton, J. A., Vizuete, W., Gold, A., & Surratt, J. D. Constraining condensed-phase formation kinetics of secondary organic aerosol components from isoprene epoxydiols. *Atmos. Chem. Phys., 16*(3), 1245-1254. doi:10.5194/acp-16-1245-2016 (2016).

Riva, M., Bell, D. M., Hansen, A.-M. K., Drozd, G. T., Zhang, Z., Gold, A., Imre, D., Surratt, J. D., Glasius, M., & Zelenyuk, A. Effect of Organic Coatings, Humidity and Aerosol Acidity on Multiphase Chemistry of Isoprene Epoxydiols. *Environmental Science & Technology, 50*(11), 5580-5588. doi:10.1021/acs.est.5b06050 (2016).

Riva, M., Chen, Y., Zhang, Y., Lei, Z., Olson, N. E., Boyer, H. C., Narayan, S., Yee, L. D., Green, H. S., Cui, T., Zhang, Z., Baumann, K., Fort, M., Edgerton, E., Budisulistiorini, S. H., Rose, C. A., Ribeiro, I. O., e Oliveira, R. L., dos Santos, E. O., Machado, C. M. D., Szopa, S., Zhao, Y., Alves, E. G., de Sá, S. S., Hu, W., Knipping, E. M., Shaw, S. L., Duvoisin Junior, S., de Souza, R. A. F., Palm, B. B., Jimenez, J.-L., Glasius, M., Goldstein, A. H., Pye, H. O. T., Gold, A., Turpin, B. J., Vizuete, W., Martin, S. T., Thornton, J. A., Dutcher, C. S., Ault, A. P., & Surratt, J. D. Increasing Isoprene Epoxydiol-to-Inorganic Sulfate Aerosol Ratio Results in Extensive Conversion of Inorganic Sulfate to Organosulfur Forms: Implications for Aerosol Physicochemical Properties. *Environmental Science & Technology, 53*(15), 8682-8694. doi:10.1021/acs.est.9b01019 (2019).

Schill, G. P., & Tolbert, M. A. Heterogeneous ice nucleation on phase-separated organic-sulfate particles: effect of liquid vs. glassy coatings. *Atmos. Chem. Phys., 13*(9), 4681-4695. doi:10.5194/acp-13-4681-2013 (2013).

Schmedding, R., Ma, M., Zhang, Y., Farrell, S., Pye, H. O. T., Chen, Y., Wang, C.-T., Rasool, Q. Z., Budisulistiorini, S. H., Ault, A. P., Surratt, J. D., & Vizuete, W. α-Pinene-Derived Organic Coatings on Acidic Sulfate Aerosol Impacts Secondary Organic Aerosol Formation from Isoprene in a Box Model. *Atmospheric environment (Oxford, England : 1994), 213*, 456-462. doi:10.1016/j.atmosenv.2019.06.005 (2019).

Schmedding, R., Rasool, Q. Z., Zhang, Y., Pye, H. O. T., Zhang, H., Chen, Y., Surratt, J. D., Lopez-Hilfiker, F. D., Thornton, J. A., Goldstein, A. H., & Vizuete, W. Predicting secondary organic aerosol phase state and viscosity and its effect on multiphase chemistry in a regional-scale air quality model. *Atmos. Chem. Phys., 20*(13), 8201-8225. doi:10.5194/acp-20-8201-2020 (2020).

https://doi.org/10.5194/egusphere-2025-2253
Preprint. Discussion started: 5 August 2025
© Author(s) 2025. CC BY 4.0 License.

Schmedding, R., & Zuend, A. A thermodynamic framework for bulk–surface partitioning in finite-volume mixed organic–inorganic aerosol particles and cloud droplets. *Atmos. Chem. Phys., 23*(13), 7741-7765. doi:10.5194/acp-23-7741-2023 (2023).

Shiraiwa, M., Li, Y., Tsimpidi, A. P., Karydis, V. A., Berkemeier, T., Pandis, S. N., Lelieveld, J., Koop, T., & Pöschl, U. Global distribution of particle phase state in atmospheric secondary organic aerosols. *Nature Communications, 8*(1), 15002. doi:10.1038/ncomms15002 (2017).

Shrivastava, M., Lou, S., Zelenyuk, A., Easter, R. C., Corley, R. A., Thrall, B. D., Rasch, P. J., Fast, J. D., Massey Simonich, S. L., Shen, H., & Tao, S. Global long-range transport and lung cancer risk from polycyclic aromatic hydrocarbons shielded by coatings of organic aerosol. *Proceedings of the National Academy of Sciences, 114*(6), 1246-1251. doi:10.1073/pnas.1618475114 (2017).

Simon, H., & Bhave, P. V. Simulating the Degree of Oxidation in Atmospheric Organic Particles. *Environmental Science & Technology, 46*(1), 331-339. doi:10.1021/es202361w (2012).

Sindelarova, K., Granier, C., Bouarar, I., Guenther, A., Tilmes, S., Stavrakou, T., Müller, J. F., Kuhn, U., Stefani, P., & Knorr, W. Global data set of biogenic VOC emissions calculated by the MEGAN model over the last 30 years. *Atmos. Chem. Phys., 14*(17), 9317-9341. doi:10.5194/acp-14-9317-2014 (2014).

Song, M., Ham, S., Andrews, R. J., You, Y., & Bertram, A. K. Liquid–liquid phase separation in organic particles containing one and two organic species: importance of the average O : C. *Atmos. Chem. Phys., 18*(16), 12075-12084. doi:10.5194/acp-18-12075-2018 (2018).

Surratt, J. D., Chan, A. W. H., Eddingsaas, N. C., Chan, M., Loza, C. L., Kwan, A. J., Hersey, S. P., Flagan, R. C., Wennberg, P. O., & Seinfeld, J. H. Reactive intermediates revealed in secondary organic aerosol formation from isoprene. *Proceedings of the National Academy of Sciences, 107*(15), 6640-6645. doi:10.1073/pnas.0911114107 (2010).

Szopa, S., V. Naik, B. A., P. Artaxo, T. Berntsen, W.D. Collins, S. Fuzzi, L. Gallardo, A. Kiendler-Scharr, Z. Klimont, H. Liao, N. Unger, & Zanis, P. (2023). 2021: Short-lived Climate Forcers. In Masson-Delmotte, P. Z. V., A. Pirani, S.L. Connors, C. Péan, S. Berger, N. Caud, Y. Chen, L. Goldfarb, M.I. Gomis, M. Huang, K. Leitzell, E. Lonnoy, J.B.R. Matthews, T.K. Maycock, T. Waterfield, O. Yelekçi, R. Yu, & B. Zhou (Eds.), *Climate Change 2021 – The Physical Science Basis: Working Group I Contribution to the Sixth Assessment Report of the Intergovernmental Panel on Climate Change* (pp. 817-922). Cambridge: Cambridge University Press.

Tammann, G., & Hesse, W. Die Abhängigkeit der Viscosität von der Temperatur bie unterkühlten Flüssigkeiten. *Zeitschrift für anorganische und allgemeine Chemie, 156*(1), 245-257. doi:https://doi.org/10.1002/zaac.19261560121 (1926).

Tong, H., Lakey, P. S. J., Arangio, A. M., Socorro, J., Kampf, C. J., Berkemeier, T., Brune, W. H., Pöschl, U., & Shiraiwa, M. Reactive oxygen species formed in aqueous mixtures of secondary organic aerosols and mineral dust influencing cloud chemistry and public health in the Anthropocene. *Faraday Discussions, 200*(0), 251-270. doi:10.1039/C7FD00023E (2017).

Ulbrich, I. M., Canagaratna, M. R., Zhang, Q., Worsnop, D. R., & Jimenez, J. L. Interpretation of organic components from Positive Matrix Factorization of aerosol mass spectrometric data. *Atmos. Chem. Phys., 9*(9), 2891-2918. doi:10.5194/acp-9-2891-2009 (2009).

Vepsäläinen, S., Calderón, S. M., Malila, J., & Prisle, N. L. Comparison of six approaches to predicting droplet activation of surface active aerosol – Part 1: moderately surface active organics. *Atmos. Chem. Phys., 22*(4), 2669-2687. doi:10.5194/acp-22-2669-2022 (2022).

Vogel, H. Das Temperaturabhangigkeitsgesetz der Viskositat von Flussigkeiten. *Phys. Z., 22*, 645-646. Retrieved from https://ci.nii.ac.jp/naid/10004192038/en/(1921).

Wagner, R., Möhler, O., Saathoff, H., Schnaiter, M., Skrotzki, J., Leisner, T., Wilson, T. W., Malkin, T. L., & Murray, B. J. Ice cloud processing of ultra-viscous/glassy aerosol particles leads to enhanced ice nucleation ability. *Atmos. Chem. Phys., 12*(18), 8589-8610. doi:10.5194/acp-12-8589-2012 (2012).

Wang, K., Zhang, Y., Yu, S., Wong, D. C., Pleim, J., Mathur, R., Kelly, J. T., & Bell, M. A comparative study of two-way and offline coupled WRF v3.4 and CMAQ v5.0.2 over the contiguous US: performance evaluation and impacts of chemistry–meteorology feedbacks on air quality. *Geosci. Model Dev., 14*(11), 7189-7221. doi:10.5194/gmd-14-7189-2021 (2021).

Wolf, M. J., Zhang, Y., Zawadowicz, M. A., Goodell, M., Froyd, K., Freney, E., Sellegri, K., Rösch, M., Cui, T., Winter, M., Lacher, L., Axisa, D., DeMott, P. J., Levin, E. J. T., Gute, E., Abbatt, J., Koss, A., Kroll, J. H., Surratt, J. D., & Cziczo,

https://doi.org/10.5194/egusphere-2025-2253
Preprint. Discussion started: 5 August 2025
© Author(s) 2025. CC BY 4.0 License.

D. J. A biogenic secondary organic aerosol source of cirrus ice nucleating particles. *Nature Communications, 11*(1), 4834. doi:10.1038/s41467-020-18424-6 (2020).

Wong, D. C., Pleim, J., Mathur, R., Binkowski, F., Otte, T., Gilliam, R., Pouliot, G., Xiu, A., Young, J. O., & Kang, D. WRF-CMAQ two-way coupled system with aerosol feedback: software development and preliminary results. *Geosci. Model Dev., 5*(2), 299-312. doi:10.5194/gmd-5-299-2012 (2012).

Xie, Y., Paulot, F., Carter, W. P. L., Nolte, C. G., Luecken, D. J., Hutzell, W. T., Wennberg, P. O., Cohen, R. C., & Pinder, R. W. Understanding the impact of recent advances in isoprene photooxidation on simulations of regional air quality. *Atmos. Chem. Phys., 13*(16), 8439-8455. doi:10.5194/acp-13-8439-2013 (2013).

Yan, J., Zhang, Y., Chen, Y., Armstrong, N. C., Buchenau, N. A., Lei, Z., Xiao, Y., Zhang, Z., Lambe, A. T., Chan, M. N., Turpin, B. J., Gold, A., Ault, A. P., & Surratt, J. D. Kinetics and Products of Heterogeneous Hydroxyl Radical Oxidation of Isoprene Epoxydiol-Derived Secondary Organic Aerosol. *ACS Earth and Space Chemistry, 7*(10), 1916-1928. doi:10.1021/acsearthspacechem.3c00073 (2023).

You, Y., Renbaum-Wolff, L., & Bertram, A. K. Liquid–liquid phase separation in particles containing organics mixed with ammonium sulfate, ammonium bisulfate, ammonium nitrate or sodium chloride. *Atmos. Chem. Phys., 13*(23), 11723-11734. doi:10.5194/acp-13-11723-2013 (2013).

You, Y., Smith, M. L., Song, M., Martin, S. T., & Bertram, A. K. Liquid–liquid phase separation in atmospherically relevant particles consisting of organic species and inorganic salts. *International Reviews in Physical Chemistry, 33*(1), 43-77. doi:10.1080/0144235X.2014.890786 (2014).

Zhang, H., Yee, L. D., Lee, B. H., Curtis, M. P., Worton, D. R., Isaacman-VanWertz, G., Offenberg, J. H., Lewandowski, M., Kleindienst, T. E., Beaver, M. R., Holder, A. L., Lonneman, W. A., Docherty, K. S., Jaoui, M., Pye, H. O. T., Hu, W., Day, D. A., Campuzano-Jost, P., Jimenez, J. L., Guo, H., Weber, R. J., de Gouw, J., Koss, A. R., Edgerton, E. S., Brune, W., Mohr, C., Lopez-Hilfiker, F. D., Lutz, A., Kreisberg, N. M., Spielman, S. R., Hering, S. V., Wilson, K. R., Thornton, J. A., & Goldstein, A. H. Monoterpenes are the largest source of summertime organic aerosol in the southeastern United States. *Proceedings of the National Academy of Sciences, 115*(9), 2038-2043. doi:10.1073/pnas.1717513115 (2018a).

Zhang, J., Shrivastava, M., Zelenyuk, A., Zaveri, R. A., Surratt, J. D., Riva, M., Bell, D., & Glasius, M. Observationally Constrained Modeling of the Reactive Uptake of Isoprene-Derived Epoxydiols under Elevated Relative Humidity and Varying Acidity of Seed Aerosol Conditions. *ACS Earth and Space Chemistry, 7*(4), 788-799. doi:10.1021/acsearthspacechem.2c00358 (2023).

Zhang, J., Wang, Y., Teng, X., Liu, L., Xu, Y., Ren, L., Shi, Z., Zhang, Y., Jiang, J., Liu, D., Hu, M., Shao, L., Chen, J., Martin, S. T., Zhang, X., & Li, W. Liquid-liquid phase separation reduces radiative absorption by aged black carbon aerosols. *Communications Earth & Environment, 3*(1), 128. doi:10.1038/s43247-022-00462-1 (2022).

Zhang, Y., Chen, Y., Lambe, A. T., Olson, N. E., Lei, Z., Craig, R. L., Zhang, Z., Gold, A., Onasch, T. B., Jayne, J. T., Worsnop, D. R., Gaston, C. J., Thornton, J. A., Vizuete, W., Ault, A. P., & Surratt, J. D. Effect of the Aerosol-Phase State on Secondary Organic Aerosol Formation from the Reactive Uptake of Isoprene-Derived Epoxydiols (IEPOX). *Environmental Science & Technology Letters, 5*(3), 167-174. doi:10.1021/acs.estlett.8b00044 (2018b).

Zhang, Y., Chen, Y., Lei, Z., Olson, N. E., Riva, M., Koss, A. R., Zhang, Z., Gold, A., Jayne, J. T., Worsnop, D. R., Onasch, T. B., Kroll, J. H., Turpin, B. J., Ault, A. P., & Surratt, J. D. Joint Impacts of Acidity and Viscosity on the Formation of Secondary Organic Aerosol from Isoprene Epoxydiols (IEPOX) in Phase Separated Particles. *ACS Earth and Space Chemistry, 3*(12), 2646-2658. doi:10.1021/acsearthspacechem.9b00209 (2019a).

Zhang, Y., Katira, S., Lee, A., Lambe, A. T., Onasch, T. B., Xu, W., Brooks, W. A., Canagaratna, M. R., Freedman, A., Jayne, J. T., Worsnop, D. R., Davidovits, P., Chandler, D., & Kolb, C. E. Kinetically controlled glass transition measurement of organic aerosol thin films using broadband dielectric spectroscopy. *Atmos. Meas. Tech., 11*(6), 3479-3490. doi:10.5194/amt-11-3479-2018 (2018).

Zhang, Y., Nichman, L., Spencer, P., Jung, J. I., Lee, A., Heffernan, B. K., Gold, A., Zhang, Z., Chen, Y., Canagaratna, M. R., Jayne, J. T., Worsnop, D. R., Onasch, T. B., Surratt, J. D., Chandler, D., Davidovits, P., & Kolb, C. E. The Cooling Rate- and Volatility-Dependent Glass-Forming Properties of Organic Aerosols Measured by Broadband Dielectric Spectroscopy. *Environmental Science & Technology, 53*(21), 12366-12378. doi:10.1021/acs.est.9b03317 (2019).

Zhang, Y., Nichman, L., Spencer, P., Jung, J. I., Lee, A., Heffernan, B. K., Gold, A., Zhang, Z., Chen, Y., Canagaratna, M. R., Jayne, J. T., Worsnop, D. R., Onasch, T. B., Surratt, J. D., Chandler, D., Davidovits, P., & Kolb, C. E. The Cooling

https://doi.org/10.5194/egusphere-2025-2253
Preprint. Discussion started: 5 August 2025
© Author(s) 2025. CC BY 4.0 License.

Rate- and Volatility-Dependent Glass-Forming Properties of Organic Aerosols Measured by Broadband Dielectric Spectroscopy. *Environmental Science & Technology, 53*(21), 12366-12378. doi:10.1021/acs.est.9b03317 (2019b).

Zhang, Z., Li, Y., Ran, H., An, J., Qu, Y., Zhou, W., Xu, W., Hu, W., Xie, H., Wang, Z., Sun, Y., & Shiraiwa, M. Simulated phase state and viscosity of secondary organic aerosols over China. *Atmos. Chem. Phys., 24*(8), 4809-4826. doi:10.5194/acp-24-4809-2024 (2024).

Zuend, A., & Seinfeld, J. H. Modeling the gas-particle partitioning of secondary organic aerosol: the importance of liquid-liquid phase separation. *Atmos. Chem. Phys., 12*(9), 3857-3882. doi:10.5194/acp-12-3857-2012 (2012).